Research Paper

Geosphere, published online on 27 August 2015 as doi:10.1130/GES01167.1

GEOSPHERE

GEOSPHERE; v. 11, no. 5

doi:10.1130/GES01167.1

11 figures; 2 tables

CORRESPONDENCE: rdorsey@uoregon.edu

CITATION: Dorsey, R.J., and Langenheim, V.E., 2015, Crustal-scale tilting of the central Salton block, southern California: Geosphere, v. 11, no. 5, doi:10.1130/GES01167.1.

Received 27 December 2014
Revision received 9 June 2015
Accepted 17 July 2015

Crustal-scale tilting of the central Salton block, southern California

Rebecca J. Dorsey[1] and Victoria E. Langenheim[2]

[1]Department of Geological Sciences, 1272 University of Oregon, Eugene, Oregon 97403-1272, USA
[2]U.S. Geological Survey, MS 989, 345 Middlefield Road, Menlo Park, California 94025, USA

ABSTRACT

The southern San Andreas fault system (California, USA) provides an excellent natural laboratory for studying the controls on vertical crustal motions related to strike-slip deformation. Here we present geologic, geomorphic, and gravity data that provide evidence for active northeastward tilting of the Santa Rosa Mountains and southern Coachella Valley about a horizontal axis oriented parallel to the San Jacinto and San Andreas faults. The Santa Rosa fault, a strand of the San Jacinto fault zone, is a large southwest-dipping normal fault on the west flank of the Santa Rosa Mountains that displays well-developed triangular facets, narrow footwall canyons, and steep hanging-wall alluvial fans. Geologic and geomorphic data reveal ongoing footwall uplift in the southern Santa Rosa Mountains, and gravity data suggest total vertical separation of ~5.0–6.5 km from the range crest to the base of the Clark Valley basin. The northeast side of the Santa Rosa Mountains has a gentler topographic gradient, large alluvial fans, no major active faults, and tilted inactive late Pleistocene fan surfaces that are deeply incised by modern upper fan channels. Sediments beneath the Coachella Valley thicken gradually northeast to a depth of ~4–5 km at an abrupt boundary at the San Andreas fault. These features all record crustal-scale tilting to the northeast that likely started when the San Jacinto fault zone initiated ca. 1.2 Ma. Tilting appears to be driven by oblique shortening and loading across a northeast-dipping southern San Andreas fault, consistent with the results of a recent boundary-element modeling study.

INTRODUCTION

The structural architecture and displacement histories of strike-slip fault zones provide insights into accumulation of three-dimensional (3-D) strain through time at transform plate boundaries. Rapid vertical motions of narrow (~0.5–5 km wide) fault slivers commonly are driven by translation of crust through small-scale geometric complexities in strike-slip fault zones (Wilcox et al., 1973; Aksu et al., 2000; McClay and Bonora, 2001; Spotila et al., 2001, 2002; Mann, 2007; Gueguen et al., 2010; Cooke et al., 2013). Vertical motions also result from tilting of larger (~10–100 km wide) strike-slip fault-bounded crustal blocks. Large-scale tilting toward strike-slip faults has been proposed to result from transform-normal extension due to rotation of principal stresses on weak strike-slip faults (Ben Avraham and Zoback, 1992). Horizontal axis tilting in transtensional strike-slip basins can occur as a result of plate motions reoriented by continental collision and escape tectonics (Mann, 1997), and translation of crust through large bends in a master strike-slip fault (Cormier et al., 2006; Sorichetta et al., 2010). In general, the causes of large-scale crustal tilting in strike-slip fault zones remain little-studied and poorly understood.

The San Andreas fault (SAF) system in southern California provides an excellent natural laboratory for the study of vertical crustal motions and tilt patterns associated with active strike-slip faulting. The geologic history is well studied, rocks and fault zones are well exposed, and the area contains a rich sedimentary archive that records changes in fault kinematics and vertical displacements through time. The Salton block (Meade and Hager, 2005; Fay and Humphreys, 2005, 2006) is a relatively intact crustal block bounded by active strands of the SAF on the northeast and the San Jacinto fault zone (SJFZ) on the southwest (Fig. 1). It occupies a structural transition from zones of active transpression along strike to the northwest in San Gorgonio Pass, to oblique dilation in the Salton Sea to the southeast (Fig. 1). Modern motions of fault-bounded crustal blocks as measured with global positioning system (GPS) are generally parallel to major strike-slip faults with a small angle of oblique convergence across the SAF in Coachella Valley (Bennett et al., 1996; Plattner et al., 2007; DeMets et al., 2010; Spinler et al., 2010). Geomorphic features and eroding Pleistocene sediments provide evidence for active uplift and erosion. The age of the SJFZ, and thus the Salton block, is known from multiple stratigraphic and structural analyses to be ca. 1.3–1.1 Ma (Morton and Matti, 1993; Matti and Morton, 1993; Lutz et al., 2006; Kirby et al., 2007; Steely et al., 2009; Janecke et al., 2010).

Recent debate has focused on the dip of the southern SAF in the Coachella Valley and Salton Trough. Historically, geophysical models have assumed a vertical dip on the fault (e.g., Meade and Hager, 2005; Smith-Konter and Sandwell, 2009; Loveless and Meade, 2011; Herbert and Cooke, 2012; Luo and Liu, 2012; Nicholson et al., 2013). Other studies suggest that the active Coachella segment of the SAF dips 60°–70° northeast based on seismicity patterns, aeromagnetic data, and modern strain documented with GPS and interferometric synthetic aperture radar (Lin et al., 2007; Fuis et al., 2012a; Lin, 2013; Lindsey and Fialko, 2013). The hypothesis for a steeply northeast-dipping SAF in this area is supported by a recent 3-D boundary-element modeling study that tested alternative fault geometries using comparison of model results to geologic evidence for vertical surface displacements around the Coachella Valley (Fattaruso et al., 2014). Debate over the dip on the southern SAF highlights the need for improved understanding of vertical motions in strike-slip fault

Geosphere, published online on 27 August 2015 as doi:10.1130/GES01167.1

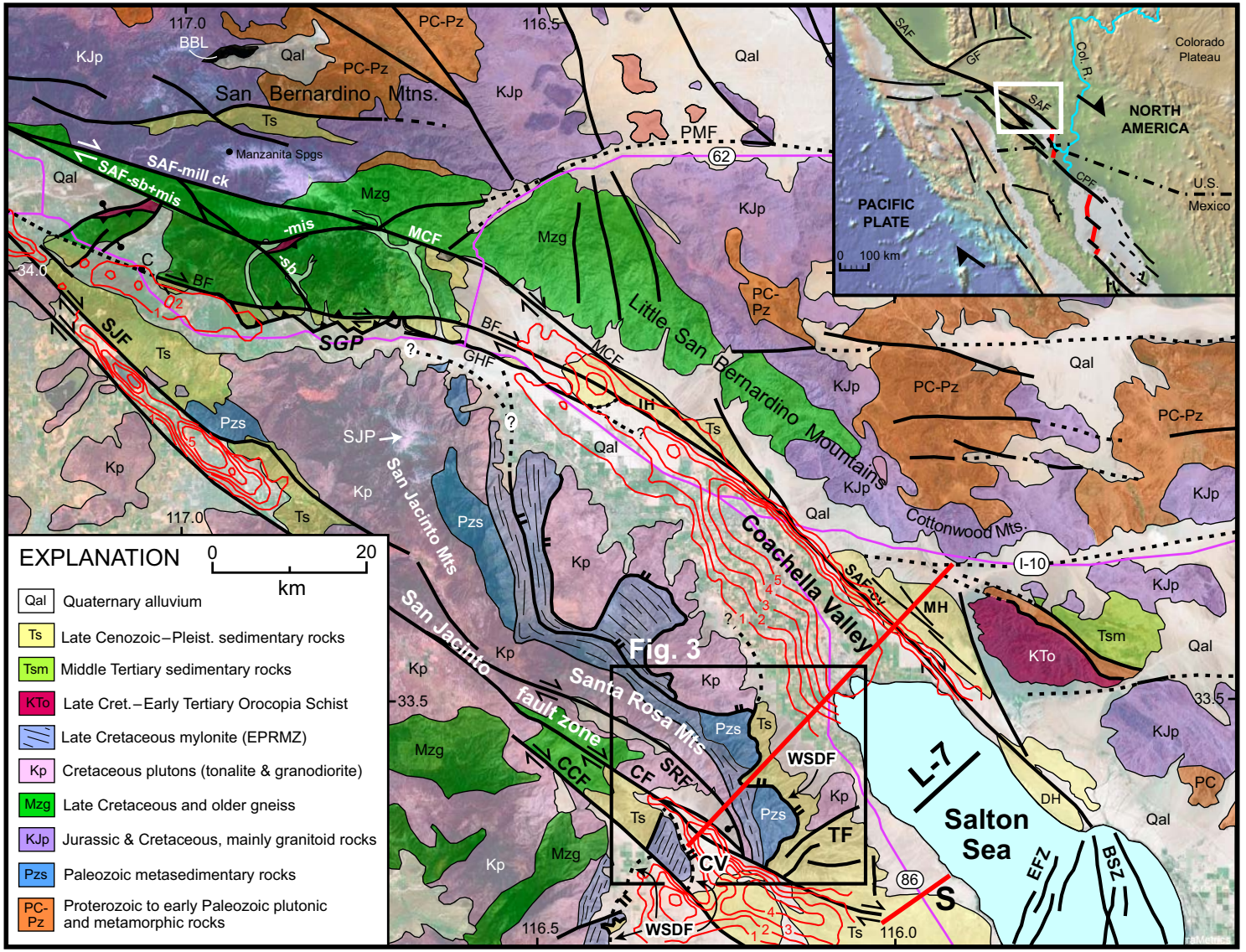

Figure 1. Geologic map of the San Andreas and San Jacinto fault zones, southern California (compiled from Jennings, 1977; Bortugno and Spittler, 1986; Matti et al., 1992; Powell, 1993; Axen and Fletcher, 1998; Janecke et al., 2010). Thin red lines are contours of subsurface sediment thickness (km) from Langenheim et al. (2005) and this study. Wide red line is line of cross section in Figure 10. Black line labeled L-7 is seismic reflection line 7 (Kell et al., 2012; Fuis et al., 2012b, 2012c). Red line labeled S is seismic reflection line of Severson (1987). Abbreviations: BBL—Big Bear Lake; BF—Banning fault; BSZ—Brawley seismic zone; C—Calimesa; CF—Clark fault; CCF—Coyote Creek fault; CPF—Cerro Prieto fault; CV—Clark Valley; -cv—Coachella Valley strand of San Andreas fault (SAF); DH—Durmid Hill; EFZ—Extra fault zone; EPRMZ—Eastern Peninsular Ranges mylonite zone; GF—Garlock fault; GHF—Garnet Hill fault; IH—Indio Hills; MCF and -mis—Mission Creek fault; MH—Mecca Hills; PMF—Pinto Mountain fault; -sb—San Bernardino strand of SAF; SGP—San Gorgonio Pass; SJF—San Jacinto fault; SJP—San Jacinto Peak; SRF—Santa Rosa fault; TF—Travertine fault; WSDF—West Salton detachment fault; Pleist.—Pleistocene; Cret.—Cretaceous.

Geosphere, published online on 27 August 2015 as doi:10.1130/GES01167.1

zones over geologic time scales (~1–2 m.y.), which offers a useful tool for testing alternative models and improving seismic hazard predictions.

This paper presents a study of crustal structure and late Quaternary to modern vertical deformation in the Santa Rosa Mountains and southern Coachella Valley, in the central part of the Salton block (Fig. 1). We integrate geologic, geomorphic, and geophysical data to interpret the geometry and timing of mountain range uplift and basin subsidence associated with strike-slip deformation. We find that since initiation of the SJFZ ca. 1.2 Ma, the central Salton block has undergone progressive northeastward tilting between the San Jacinto and southern San Andreas faults. We consider several mechanisms that could drive this pattern of crustal tilting, and find that it is best explained by a small angle of oblique convergence and crustal loading across a steeply northeast-dipping southern SAF.

GEOLOGIC AND TECTONIC SETTING

The southern SAF system (Fig. 1) is a network of dextral and oblique-slip faults that record a complex history of late Cenozoic transtensional and transpressional deformation (e.g., Crowell, 1974, 1981; Ehlig, 1981; Matti and Morton, 1993; Powell, 1993; Weldon et al., 1993; Darin and Dorsey, 2013). The SAF in Coachella Valley consists of a single main strand in the southeast that splits into the Banning and Mission Creek faults in the northwest (Fig. 1). The fault zone contains abundant geomorphic signs of recent and ongoing deformation, including dextrally deflected and beheaded streams, shutter ridges, sag ponds, fault scarps, and displaced Quaternary and Holocene alluvial fans (e.g., Keller et al., 1982; Sieh and Williams, 1990; Shifflett et al., 2002; Behr et al., 2010; Gray et al., 2014). Modeling of GPS data suggests that slip rates decrease northward from ~23 mm/yr in the southernmost Coachella Valley to ~14–18 mm/yr in the northern Coachella Valley (Spinler et al., 2010; Behr et al., 2010). Geologic structures and stratigraphy in the Mecca Hills record Pleistocene to modern transpression and fault-normal shortening in a narrow belt northeast of the SAF (Fig. 1; Sylvester and Smith, 1976, 1987; Rymer, 1991, 1994; Sheridan and Weldon, 1994; McNabb, 2013). The restraining bend in San Gorgonio Pass (Fig. 1) is a zone of active transpressional deformation, crustal thickening, and high topography (Matti et al., 1985, 1992; Harden and Matti, 1989; Spotila and Sieh, 2000; Yule and Sieh, 2003). The SAF zone on the north side of San Gorgonio Pass is a network of dextral-reverse faults with an overall north dip revealed by seismology (Yule and Sieh, 2003; Carena et al., 2004) and gravity and magnetic data (Langenheim et al., 2004, 2005), a geometry consistent with the results of 3-D numerical modeling (Dair and Cooke, 2009; Cooke and Dair, 2011; Herbert and Cooke, 2012).

The late Cenozoic tectonic history of the region is recorded in sedimentary rocks and structures exposed in zones of recent uplift around the margins of the modern valleys. Basin subsidence and deposition in the Fish Creek–Vallecito basin (western Salton Trough) began ca. 8 ± 0.5 Ma in response to regional extension and transtension associated with initiation of the southern SAF system (Dorsey et al., 2011). Late Miocene to Pleistocene crustal extension and thinning produced deep subsidence in the Salton basin and accumulation of thick nonmarine and marine deposits that are now exposed west of the Salton Sea (Winker, 1987; Winker and Kidwell, 1986, 1996; Dorsey et al., 2011). The Imperial Formation records widespread marine incursion ca. 6.3–6.5 Ma along a narrow fault-bounded marine seaway at the north end of the Gulf of California (Dibblee, 1954; Allen, 1957; Matti et al., 1992; McDougall et al., 1999; Dorsey et al., 2007). Latest Miocene to Pleistocene transtension was accommodated by combined strike-slip offset on the SAF and top-to-the-east offset on the low-angle West Salton detachment fault (WSDF), which accommodated ~8–10 km of Pliocene to early Pleistocene east-west extension and related subsidence at the western margin of the Salton Trough (Axen and Fletcher, 1998; Shirvell et al., 2009; Dorsey et al., 2011). The WSDF is a regional structure bounding a large supradetachment basin that is well mapped where the basin has been inverted by young uplift, and is inferred to be present beneath deep modern basins in the western Salton Trough and Coachella Valley where inversion has not occurred (Axen and Fletcher, 1998; Janecke et al., 2010). Regional extension and lithospheric rupture across the plate boundary have continued to the present day, resulting in rapid subsidence and accumulation of Colorado River–derived sediment in basins as much as 10–12 km deep (Fuis et al., 1984; Elders and Sass, 1988; Herzig et al., 1988; Schmitt and Vazquez, 2006; Schmitt and Hulen, 2008; Dorsey, 2010).

The SJFZ cuts obliquely across the northern Peninsular Ranges in a network of strike-slip and oblique-slip fault strands that truncate, postdate, and offset the WSDF (Fig. 1). The main strands of the SJFZ west of the Salton Sea are the Coyote Creek, Clark, and Santa Rosa faults. The Santa Rosa fault was originally identified by Dibblee (1954) and confirmed by Janecke et al. (2010). Geologic studies show that the SJFZ and related faults initiated ca. 1.3–1.1 Ma in the western Salton Trough (Lutz et al., 2006; Kirby et al., 2007; Steely et al., 2009; Janecke et al., 2010), overlapping with an age of 1.3–1.5 Ma in the northern SJFZ (Morton and Matti, 1993; Matti and Morton, 1993) and 1.2 ± 0.1 Ma for the Elsinore fault at the western edge of the Salton Trough (Dorsey et al., 2012). A slightly older age of 1.8 ± 0.5 Ma was suggested for the SJFZ based on late Pleistocene slip rates and total offset (Blisniuk et al., 2010). The younger age (1.1–1.3 Ma) is well supported by multiple lines of geologic and stratigraphic data in diverse locations (e.g., Lutz et al., 2006; Kirby et al., 2007; Steely et al., 2009). The discrepancy between published initiation ages suggests that slip rates may have slowed since fault initiation (Bennett et al., 2004), or late Pleistocene estimates may have missed some off-fault strain that is pervasive in this area (Janecke et al., 2010).

METHODS

This study integrates geologic, geomorphic, and geophysical data to interpret crustal structure, depth of basins, and patterns of Pleistocene to modern deformation. Methods include compilation of previously published and unpublished geologic maps, mapping and observations of fault-scarp morphol-

Geosphere, published online on 27 August 2015 as doi:10.1130/GES01167.1

ogy, measurement of fault-zone fabrics, quantitative geomorphic analysis in ArcMap (http://www.esri.com/software/arcgis) using 30 m digital elevation models (DEMs), and measurement of alluvial fan and corresponding catchment areas on DEMs and satellite imagery. Gravity data (Biehler et al., 1992; Langenheim et al., 2005, 2007; Martin et al., 1997; Langenheim, 2008, personal data) were used to examine basin geometry using two different methods. Depth of subsurface basins throughout the region of Figure 1 was modeled through 3-D inversion of gravity data using the method of Jachens and Moring (1990) and parameters in Langenheim et al. (2005; see following). Forward modeling (2-D) was used to examine basin and fault geometry along a profile across the central Salton block (red line in Fig. 2), assuming a density contrast of –400 kg/m^3 between the basement and basin fill. The geology at the surface places a critical constraint on both modeling methods. The gravity model does not inform on fault geometry below the basin-basement interface.

The gravity inversion and 2-D forward model take advantage of the significant density contrast between dense crystalline basement rocks and Cenozoic lower density sedimentary rocks and deposits. The method of Jachens and Moring (1990), modified to include drill hole data and other geophysical data as constraints, separates the isostatic gravity field into the component produced by variations in basement density and that caused by thick basin deposits, which is then inverted for thickness. The basement gravity field is allowed to vary laterally and is estimated by passing a surface through those values measured on basement outcrops. This field is subtracted from the isostatic gravity field to produce an initial estimate of the basin gravity. Because the basement gravity values near the basin edge are affected by the gravity effect of the low-density basin fill and thus underestimated, a forward calculation of the basin gravity field is used to correct the basement gravity measurements. This process is repeated until further steps do not result in significant changes to the modeled thickness of the basin deposits, usually in five or six steps. The basin gravity field is converted to basin thickness using an assumed density contrast that varied with depth between the basin and underlying basement (Table 1). The density-depth relationship produces basin depths and shapes that are generally consistent with those obtained by recent seismic profiling in Coachella Valley (Langenheim et al., 2012, 2013).

RESULTS

Regional Gravity and Structure

The geologic map (Fig. 1) and isostatic gravity map (Fig. 2) show the distribution of fault-bounded sediment-filled basins (gravity lows) and mountain range uplifts (gravity highs) in the southern SAF system. Total depth of the southern Coachella Valley increases gradually from the southwest, where sediments onlap crystalline and sedimentary rocks of the Santa Rosa Mountains, to the northeast where the basin is abruptly truncated at the SAF (Figs. 1 and 2). Along strike to the southeast, high gravity values at the south end of the Salton Sea indicate the presence of mafic intrusions ~12–20 km beneath a deep sediment-filled basin in the Salton Trough (Fig. 2; Fuis et al., 1984; Schmitt and Vazquez, 2006; Han et al., 2013). The gravity high at the south end of the Salton Sea is enhanced by increased density of sedimentary fill (Kasameyer and Hearst, 1988) that results from hydrothermal alteration, metamorphism, and emplacement of basaltic sills, dikes, and flows into the thick sedimentary fill. In this area, basin depth contours are not shown because of the absence of a gravity low associated with the basin.

Deep fault-bounded basins are also present within the SJFZ beneath Borrego and Clark Valleys (Figs. 1 and 2). The 3-D inversion of gravity data indicates that the subsurface Clark basin is as much as 4 km deep ~5 km southeast of Clark Lake (Fig. 3). Along a southwest-northeast cross section across the Santa Rosa Mountains and southern Coachella Valley (Figs. 1 and 2), the 3-D inversion estimates a basin thickness of ~3 km, whereas our 2-D forward model using a constant density contrast of –400 kg/m^3 indicates a depth of 4 km. The northeast margin of the basin is marked by a steep gravity gradient. The location of the Clark fault relative to the gravity gradient indicates a nearly vertical dip in Clark Valley, east and northeast of Clark Lake (Fig. 3). The Clark fault curves into a more east trend southeast of the Santa Rosa Mountains where it splays into multiple strands that define an overall restraining bend in a zone of complex active transpressional deformation (Fig. 1; Kirby et al., 2007; Belgarde, 2007; Janecke et al., 2010; Thornock, 2013).

Geology of the Santa Rosa Mountains and Clark Valley

The geologic map in Figure 3 shows major faults, sedimentary rocks, and basement units of the Santa Rosa Mountains and adjacent area. The SJFZ in this area includes the Coyote Creek, Clark, and Santa Rosa faults. The Clark fault in Clark Valley consists of two main strands: (1) a southwestern strand with a prominent surface trace that cuts the Ocotillo Formation and marks the eastern margin of Clark dry lake; and (2) a northeastern strand that is mostly covered by Quaternary alluvium but marks the eastern faulted margin of the basin at the base of steep alluvial fans (Fig. 3). A distinctive belt of Cretaceous mylonite has dextral separation of ~15–18 km across the Clark fault (Sharp, 1967; Bartholomew, 1970; Todd et al., 1988; Janecke et al., 2010). The Santa Rosa fault is a large active normal fault that bounds the steep southwestern margin of the Santa Rosa Mountains (Fig. 3; Dibblee, 1954, 1984; Janecke et al., 2010). The fault appears to be interrupted by a large Quaternary landslide in the footwall (possibly an eastward reentrant of the main fault) that coincides with a ~40° change in the trend of the range crest. The trace of the Santa Rosa fault, however, cuts the landslide, as revealed by smaller discontinuous northwest-striking fault scarps that record young offset of the inferred landslide mass. Other young faults associated with the SJFZ in this area include the northwest-striking Buck Ridge and Coyote Creek faults, unnamed normal faults on the east and west sides of Coyote Mountain, and the east-northeast–striking Travertine fault (Fig. 3).

Geosphere, published online on 27 August 2015 as doi:10.1130/GES01167.1

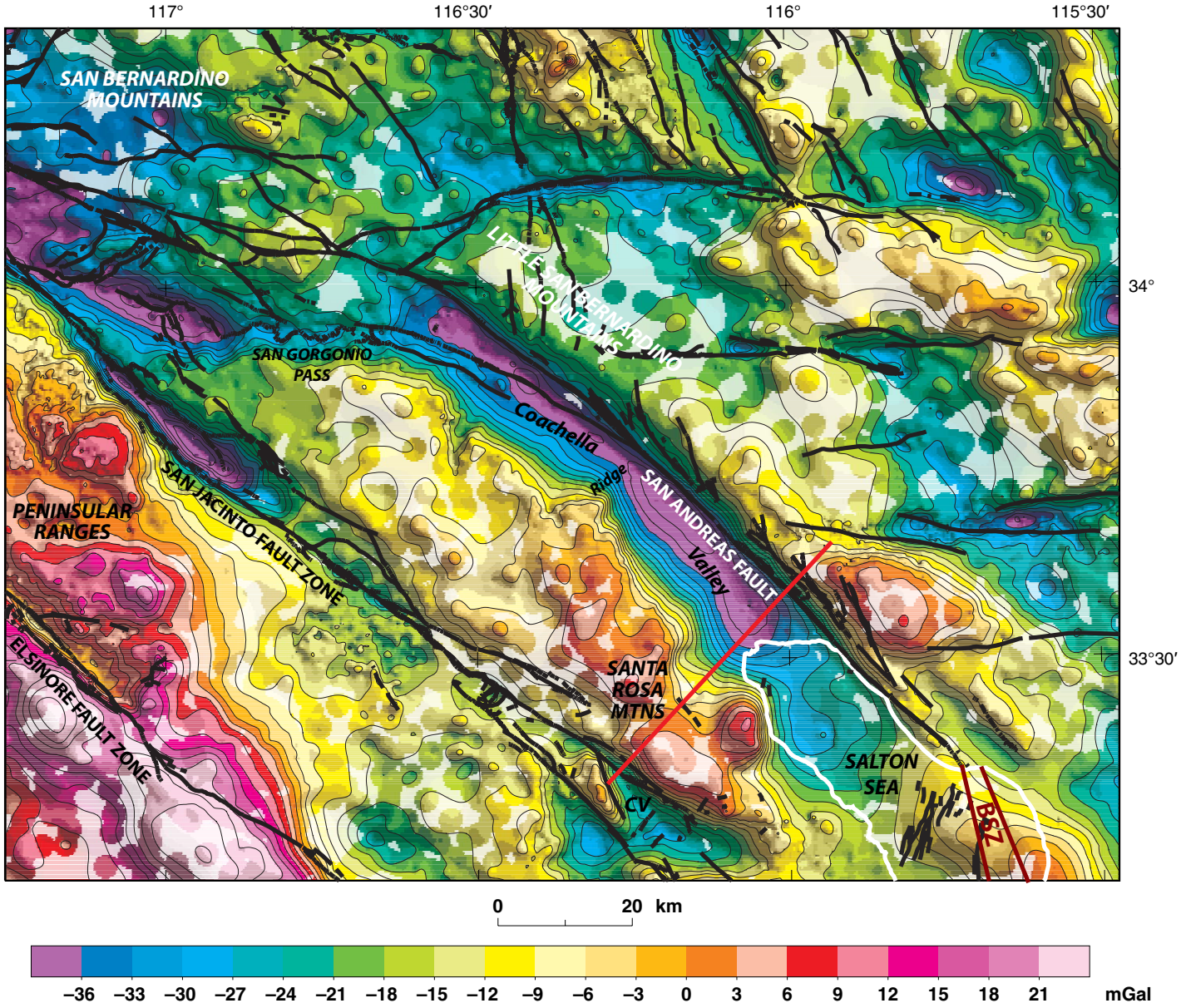

Figure 2. Isostatic gravity map of the southern San Andreas fault system. Colored areas indicate values located ≤2 km from gravity measurements; white areas are >2 km from data control points. Black lines are faults from U.S. Geological Survey and California Geological Survey (2006) and Brothers et al. (2009). Wide red line is the line of profile in Figure 10. BSZ—Brawley seismic zone; CV—Clark Valley; MTNS—mountains. Prominent gravity lows in Coachella and Clark Valleys reflect thick sedimentary deposits. Gravity high in the southern Salton Sea reflects the presence of denser basin fill due to hydrothermal alteration and mafic intrusions at depth.

Geosphere, published online on 27 August 2015 as doi:10.1130/GES01167.1

TABLE 1. DENSITY-DEPTH FUNCTION FOR CALCULATING BASIN DEPTHS

Depth range (m)	Density contrast (kg/m³)
0–100	–550
100–200	–430
200–600	–360
600–1500	–300
>1500	–230

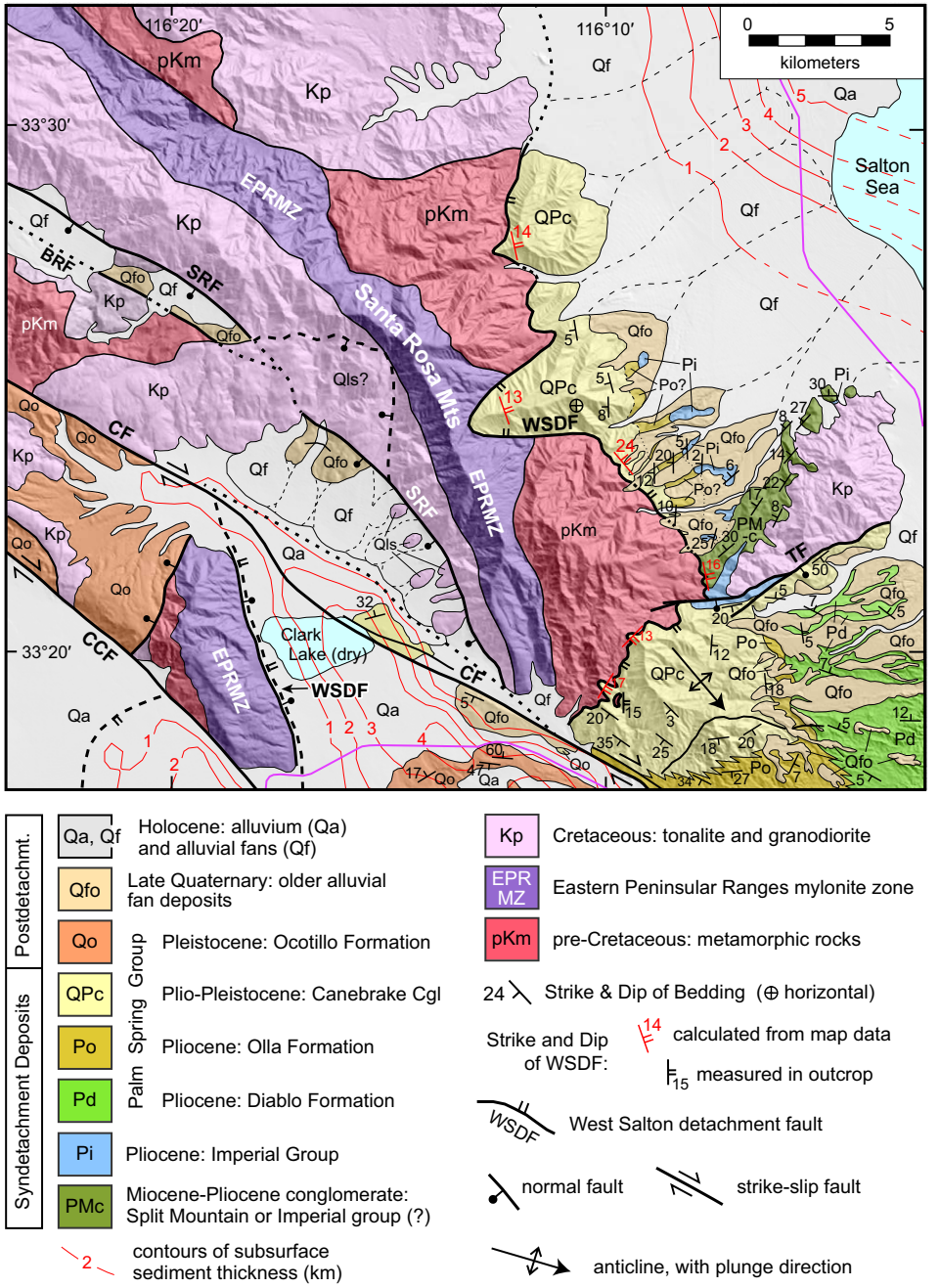

Figure 3. Geologic map of the Santa Rosa Mountains and Clark Valley area on a hillshaded digital elevation model topographic base. Compiled from Dibblee (1954, 2008), Sharp (1967), Todd et al. (1988), Dorsey (2002), Janecke et al. (2010), and Dorsey (personal map data). Contours of subsurface sediment thickness (red lines) from Figure 1. Abbreviations as in Figure 1. BRF—Buck Ridge fault; Cgl—Conglomerate; Qls?—inferred Quaternary landslide; TF—Travertine fault.

Geosphere, published online on 27 August 2015 as doi:10.1130/GES01167.1

In the Santa Rosa Mountains, the WSDF (Zosel fault of Matti et al., 2006, 2007) juxtaposes Pliocene–Pleistocene sedimentary rocks in the hanging wall against Cretaceous plutonic rocks and mylonite in the footwall (Fig. 3). This fault is reported to dip ~20° east near the range crest, steepening to >65° at lower elevations along the eastern range front (Matti et al., 2002, 2006, 2007), although our estimates based on 3-point constructions yield dips of 13°–24° (most are <20°) for the WSDF in the southern Santa Rosa Mountains. At the south end of the range (Fig. 3), a dip estimate of 17° using this method is consistent with a dip of 15° that was measured directly on the fault plane, lending support for generally low dips on the WSDF in the southern Santa Rosa Mountains. The WSDF is truncated and offset dextrally and vertically by strands of the postdetachment SJFZ, including the Clark and Santa Rosa faults (Figs. 1 and 3). These relationships show that the buried trace of the WSDF on the west side of Clark Valley was originally a southern continuation of the WSDF in the Santa Rosa Mountains, prior to dextral offset on the Clark fault.

Sediments and sedimentary rocks in the study area consist of (1) the late Miocene to early Pliocene Imperial group (nomenclature of Winker and Kidwell, 1996); (2) Pliocene-Pleistocene Palm Spring group including the Canebrake Conglomerate and Olla, Diablo, and Ocotillo formations; and (3) late Pleistocene to modern alluvial-fan and stream deposits (Fig. 3). Marine deposits and conglomerate of the Imperial group onlap onto erosional paleotopography in Cretaceous plutonic rocks on the north flank of Travertine Ridge in the southeastern Santa Rosa Mountains (Cox et al., 2002; King et al., 2002; Powell, 2008). Northwest of there, the Imperial group is overlain by a gently west-dipping, coarsening-upward sequence from fine-grained marine claystone through interbedded fossiliferous sandstone and mudstone to upward-coarsening Canebrake Conglomerate exposed at elevations to ~1400 m in the high Santa Rosa Mountains (Cox et al., 2002; King et al., 2002). King et al. (2002) reported marine deposits exposed at elevations as much as 625 m above sea level. Our map compilation indicates a slightly lower maximum elevation of ~550–600 m for marine deposits in the southeastern Santa Rosa Mountains (Fig. 3). At the south end of the range, coarse boulder Canebrake Conglomerate passes laterally to the southeast into pebbly sandstone and interbedded sandstone and mudstone of the age-equivalent Olla formation (Fig. 3).

Geomorphology

The topography of the Santa Rosa Mountains is asymmetrical and segmented into linear-trending southeast and northwest sectors (Fig. 4). In the southeast, the range crest trends N25°W and the precipitous western slope drops from 1600 m at the crest to 500 m elevation at the heads of steep alluvial fans over a distance of ~2.5 km, at an average slope of ~24°. In contrast, a similar elevation drop on the east side of the range spans a distance of ~6.3 km at an average slope of ~10° (Fig. 4A). Pronounced topographic asymmetry is also seen in the slope map (Fig. 4B), which reveals overall steeper slopes on the west side of the range and gentler slopes on the east, and topographic profiles in Figure 5. Local ridges and embayments on the northeast side of the range are produced by uplift, erosion, and cannibalization of older rocks and alluvial fan deposits. The northwest sector of the Santa Rosa Mountains trends ~N60°W and the range crest reaches elevations of >2000 m (Fig. 4). The high mountains are flanked on the southwest by the northern continuation of the Santa Rosa fault, defined by a sharp break in topography, and a high perched valley separated from Clark Lake by an east-trending ridge of Cretaceous plutonic rock (Figs. 3 and 4). Topographic asymmetry seen in the southeast is not as pronounced in the northwest sector due to the presence of the perched valley.

The southern Santa Rosa Mountains are flanked by a steep fault-bounded range front on the southwest and a lower gradient, unfaulted northeast side. The Santa Rosa fault displays abundant geomorphic features typical of active range-bounding normal faults, including steep landslide-dominated catchments in the footwall that deliver coarse sediment to small steep alluvial fans in the hanging wall (Figs. 3 and 6A). Well-developed triangular fault facets range in height from ~250 to 600 m, suggestive of active slip in the range of 0.5–2.0 mm/yr (dePolo and Anderson, 2000). Steep boulder-rich alluvial fans are faulted against pre-Tertiary crystalline rocks along a steeply southwest-dipping fault zone characterized by brittle gouge and microfaults exposed along the range front. The Santa Rosa fault exposed at the mouth of one steep canyon (inset, Fig. 6A) has a measured strike of 335° and dip of 67°SW.

The northeastern Santa Rosa Mountains display lower gradient slopes with larger, lower gradient alluvial fans compared to the southwest side (Figs. 4 and 6B). Sedimentary units in this area are divided into (1) syndetachment deposits of the Pliocene to early Pleistocene Imperial and Palm Spring groups exposed in the hanging wall of the inactive WSDF; and (2) postdetachment late Quaternary to Holocene alluvial fan deposits (Fig. 3). Marine deposits of the Imperial Formation are exposed at elevations up to 625 m above sea level (King et al., 2002), and overlying alluvial fan deposits of the Canebrake Conglomerate are exposed at elevations to 1420 m.

Postdetachment alluvial fan deposits are erosionally inset into older syndetachment deposits and display systematic age-dependent variations in morphology. Late Quaternary fans have inactive, desert-varnish surfaces and are ~0.8°–1.5° steeper than modern alluvial fans and upper fan channels (Fig. 7). Elevations of late Quaternary and modern fan surfaces diverge in the upslope direction, such that modern upper fan channels are incised as much as 70–80 m into the older, more steeply inclined late Quaternary fan surfaces. These relationships provide clear evidence for incision of older alluvial fans due to progressive northeastward tilting around a horizontal axis or fulcrum (Figs. 7 and 8). These geomorphic features are commonly observed on hanging-wall dip slopes associated with other active normal faults, and are similarly interpreted to record progressive crustal tilting (e.g., Hooke, 1972; Gawthorpe and Leeder, 2000).

Geosphere, published online on 27 August 2015 as doi:10.1130/GES01167.1

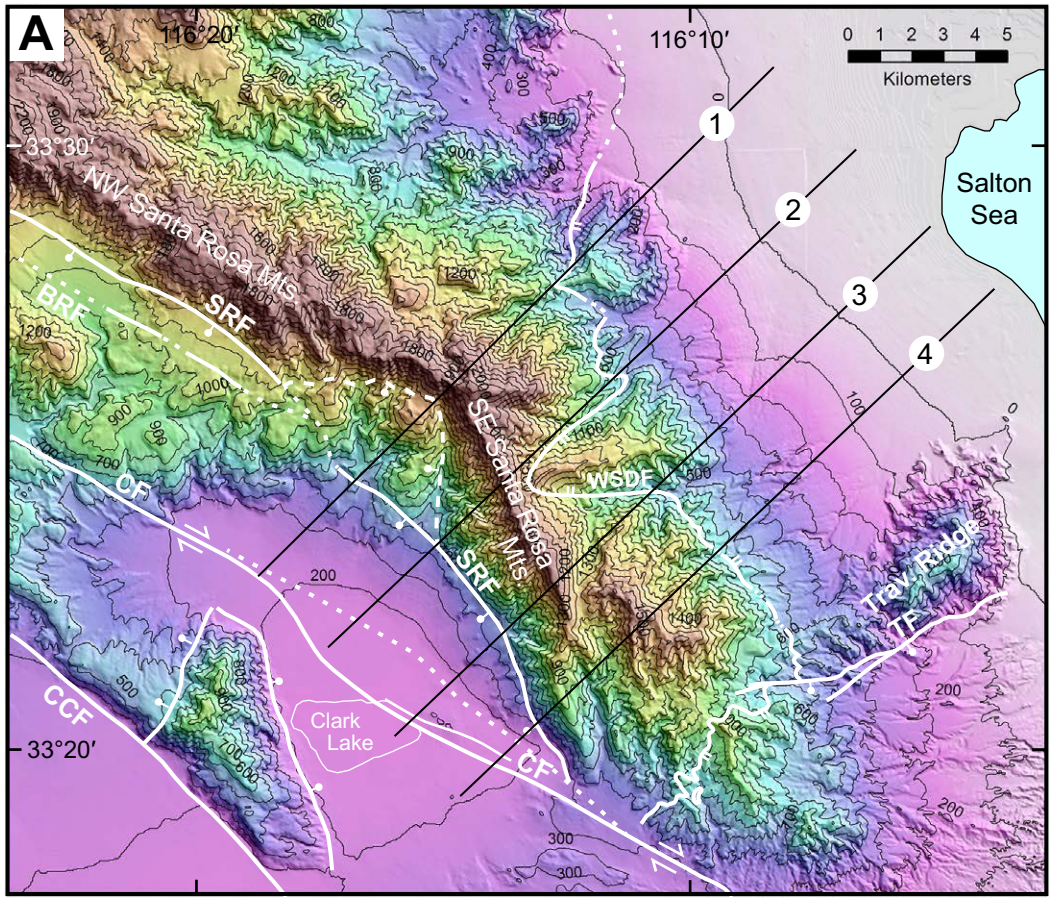

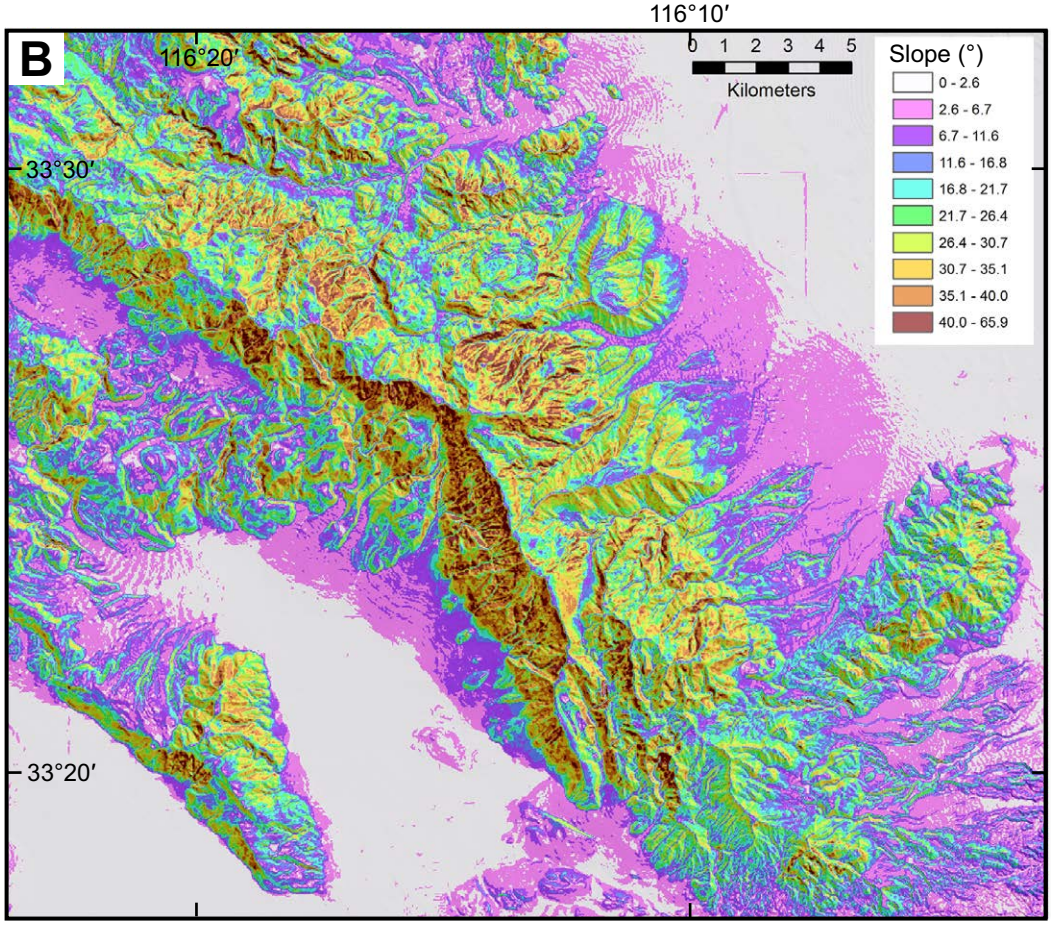

Figure 4. (A) Color digital elevation model and topographic map of the Santa Rosa Mountains and adjacent areas. Black lines labeled 1–4 are transects for topographic profiles in Figure 5. Contour interval, 100 m. Abbreviations: BRF—Buck Ridge fault; CF—Clark fault; CCF—Coyote Creek fault; SRF—Santa Rosa fault; WSDF—West Salton detachment fault; TF—Travertine fault. (B) Slope map for same area as A. Both maps reveal asymmetric topography of the Santa Rosa Mountains.

Geosphere, published online on 27 August 2015 as doi:10.1130/GES01167.1

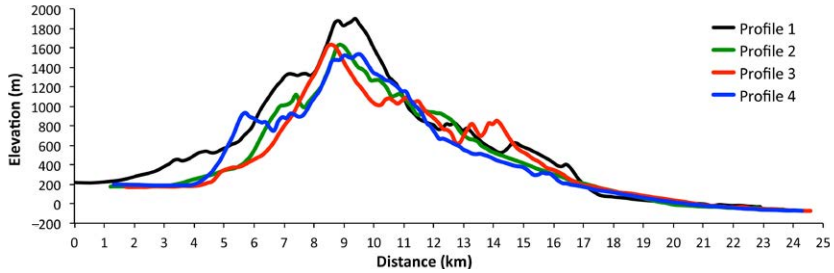

Figure 5. Topographic profiles across the southeastern Santa Rosa Mountains, showing asymmetry of the range and flanking alluvial fans. See Figure 4A for locations of profiles. Profiles are shifted horizontally to align maximum elevations in the range.

Fan Catchment Analysis

Fan catchment analysis is motivated by previous studies showing that the rate of basin subsidence exerts a primary control on the ratio of alluvial fan area (Af) to catchment area (Ac) (Whipple and Trayler, 1996; Allen and Hovius, 1998; Allen and Densmore, 2000; Dade and Verdeyen, 2007). Fast subsidence causes a greater percent of sediment to accumulate in the vertical dimension, reducing fan area for a given catchment area and generating a smaller ratio Af/Ac. Similarly, if other variables such as rock lithology and climate are held constant, slower subsidence generates a larger fan area for a given catchment size, and larger ratio Af/Ac.

Figure 8 is a shaded 30 m DEM showing modern alluvial fans and corresponding catchments in the southern Santa Rosa Mountains that were analyzed for this study. Alluvial fans with areas <~0.4 km^2 are omitted because uncertainties become large relative to measured areas. Fan areas on the southwest side of the range vary between ~0.5 and 8 km^2, and the mean Af/Ac is 0.64 ± 0.08 (1 standard error) (Table 2; Fig. 9). In contrast, modern fans on the northeast side of the range have areas of ~3–29 km^2 with an average ratio Af/Ac of 1.19 ± 0.14 (Table 2; Fig. 9). The lower Af/Ac ratios on the southwest side of the range reflect the influence of active fault offset, basin subsidence, and trapping of coarse deposits close to the Santa Rosa normal fault. In contrast, tilting about a horizontal axis (fulcrum) on the unfaulted northeast side produces relatively slow subsidence, resulting in larger alluvial fans and larger average Af/Ac (Fig. 9). These results are consistent with other evidence presented here (Figs. 6 and 7) that the southern Santa Rosa Mountains occupy a relatively intact, actively tilting crustal block bounded on its southwest by an active fault zone with significant vertical displacement.

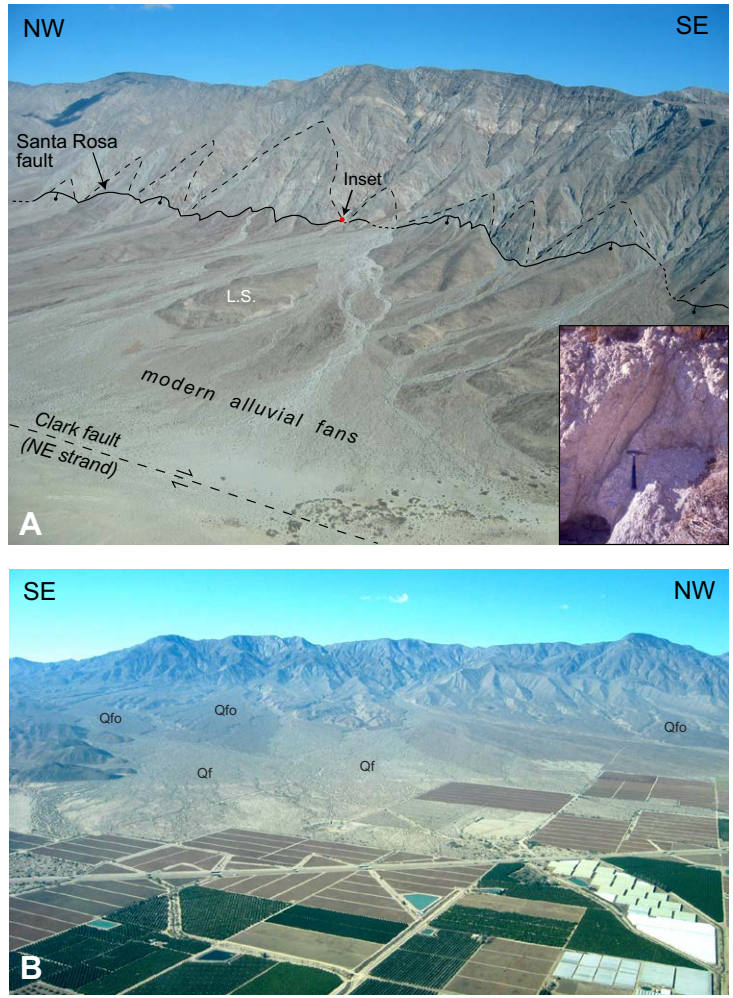

Figure 6. Comparison of geomorphic features on west and east sides of the southern Santa Rosa Mountains. (A) Oblique aerial photograph looking approximately north at steep fault-bounded western range front. The Santa Rosa fault displays classic features of an active normal fault, including triangular facets (dashed lines), steep footwall canyons, and small alluvial fans that head at the faulted base of the footwall slope. L.S.—landslide. Inset is closeup of the Santa Rosa fault showing brittle fault gouge in fractured granodiorite; fault surface strikes 335° and dips 67°SW. (B) Oblique view looking southwest at large alluvial fans on east side of the southern Santa Rosa Mountains. Qf—modern alluvial fans; Qfo—older Quaternary fans.

Geosphere, published online on 27 August 2015 as doi:10.1130/GES01167.1

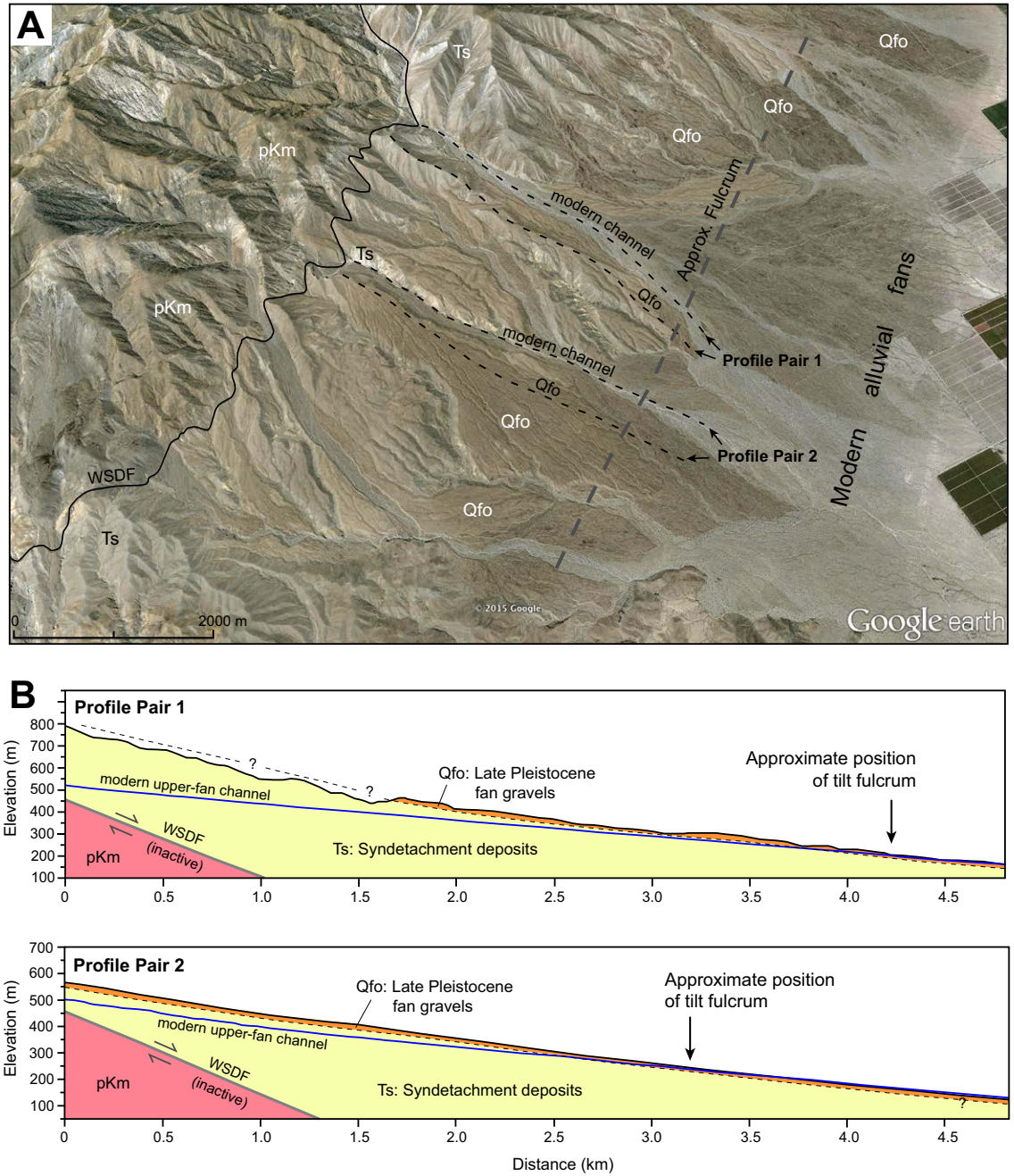

Figure 7. (A) Oblique view of the eastern Santa Rosa Mountains showing inset fan relationships. Modern upper fan channels are incised into steeper, inactive late Pleistocene alluvial fans (Qfo), which are erosionally inset into older Pliocene–Pleistocene syndetachment deposits (Ts) (pKm—pre-Cretaceous metamorphic rocks). WSDF—West Salton detachment fault. (B) Two pairs of topographic profiles showing the lower slope of modern upper fan channels that are incised into steeper, inactive late Pleistocene fan surfaces. These features record active tilting to the northeast.

Geosphere, published online on 27 August 2015 as doi:10.1130/GES01167.1

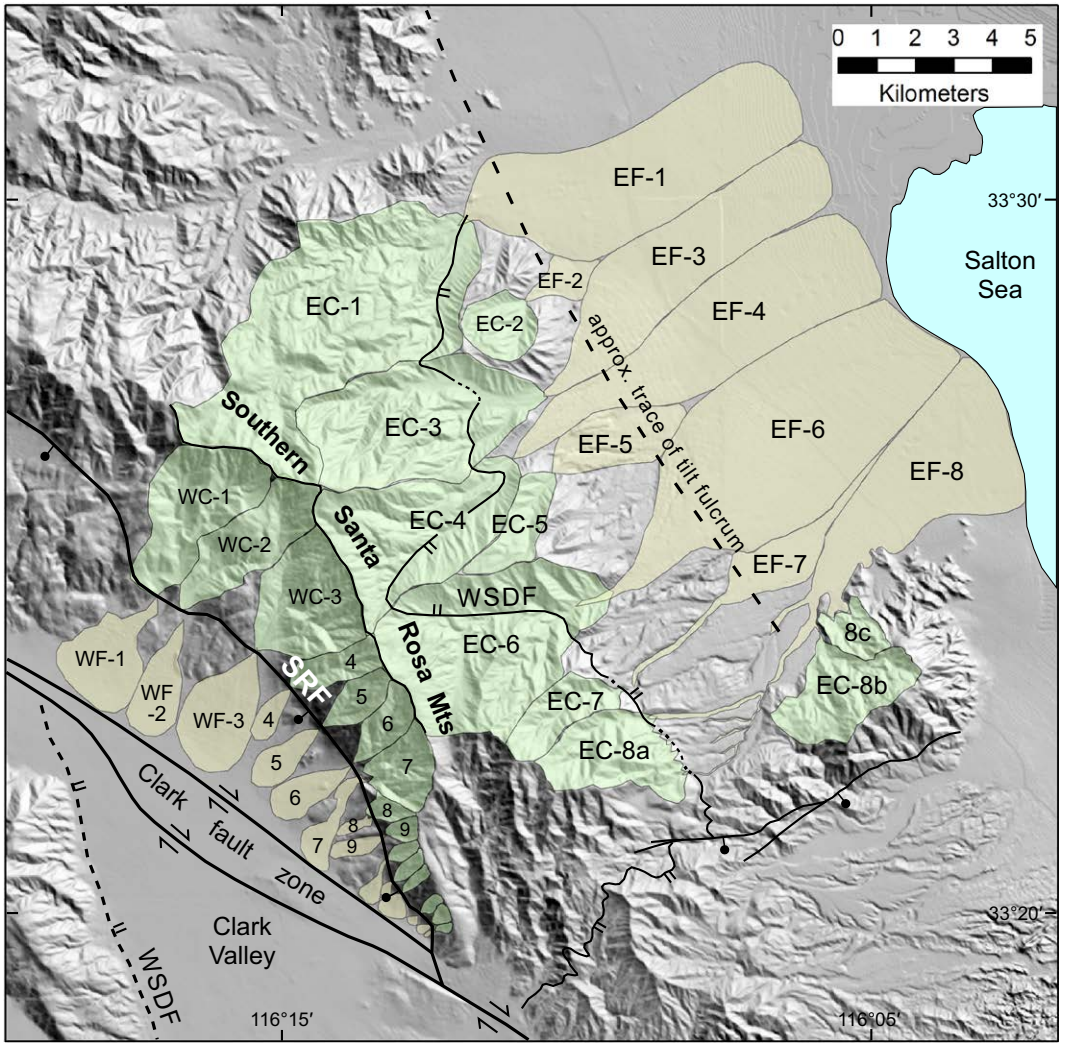

Figure 8. Shaded relief map showing outline of alluvial fans and corresponding catchments used to calculate fan catchment ratios for the west and east sides of the Santa Rosa Mountains. EC—eastern catchments; EF—eastern fans; WC—western catchments; WF—western fans; WSDF—West Salton detachment fault; SRF—Santa Rosa fault. Numbers correspond to pair numbers in Table 2, and results are shown in Figure 9.

Structural Cross Section

The cross section in Figure 10 shows interpreted crustal structure along a transect from the SJFZ in the southwest to the SAF in the northeast, constrained by surface geology, gravity data, and field observations summarized here. Splaying active strands of the SJFZ (Clark and Santa Rosa faults) define a transtensional negative flower structure that bounds a sediment-filled basin 3–4 km deep in Clark Valley. This style of oblique offset is common in transtensional strike-slip fault zones, where basins subside in response to active fault-controlled oblique dilation (e.g., Aksu et al., 2000; Mann, 2007). We infer that the sediment-basement contact beneath Clark Valley is a truncated segment of the inactive WSDF based on the mapped trace of the WSDF along the western edge of Clark Valley (Figs. 1 and 3; Axen and Fletcher, 1998; Janecke et al., 2010). The amount of extension on the WSDF is not known from the Santa Rosa Mountains, but is estimated to be ~8–10 km in the Pinyon Ridge area southwest of Clark Valley (Shirvell et al., 2009).

Geosphere, published online on 27 August 2015 as doi:10.1130/GES01167.1

TABLE 2. AREAS OF ALLUVIAL FANS AND CATCHMENTS, AND FAN:CATCHMENT RATIOS

Pair #	Catchment area (km^2)	Fan area (km^2)	Fan:catchment ratio
West side of southern Santa Rosa Mountains			
1	7.87	4.26	0.54
2	5.63	2.49	0.44
3	6.97	4.49	0.64
4	1.88	0.68	0.36
5	1.53	1.33	0.87
6	1.70	1.53	0.90
7	2.64	1.26	0.48
8	0.53	0.22	0.41
9	0.41	0.44	1.07
East side of southern Santa Rosa Mountains			
1	29.30	22.40	0.77
2	2.61	1.33	0.51
3	15.50	15.60	1.01
4	12.70	19.40	1.53
5	2.83	4.35	1.54
6	18.80	31.20	1.66
7	3.32	4.21	1.27
8	13.77	16.80	1.22

Note: West side mean = 0.64, standard error = 0.08. East side mean = 1.19, standard error = 0.14.

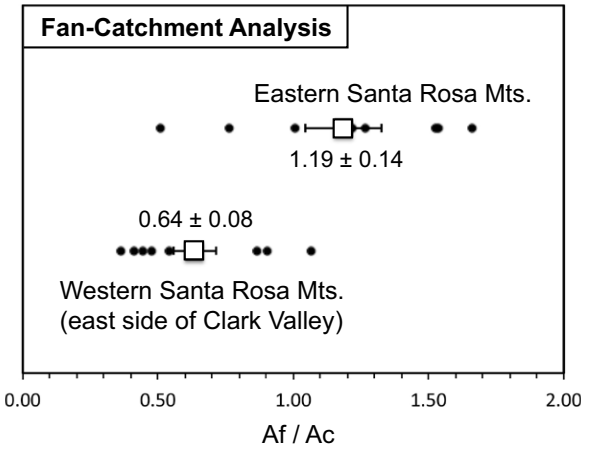

Figure 9. Plot of fan area/catchment area (Af/Ac) for the west and east sides of the southern Santa Rosa Mountains (Mts.) (Fig. 8). Smaller fan/catchment ratios in the west reflect the influence of subsidence on the Santa Rosa fault. Eastward tilting in the footwall of the fault and the absence of an active fault in the east contribute to larger Af/Ac ratios in the east. Values shown are the mean and standard error for the two groups of fan catchment pairs.

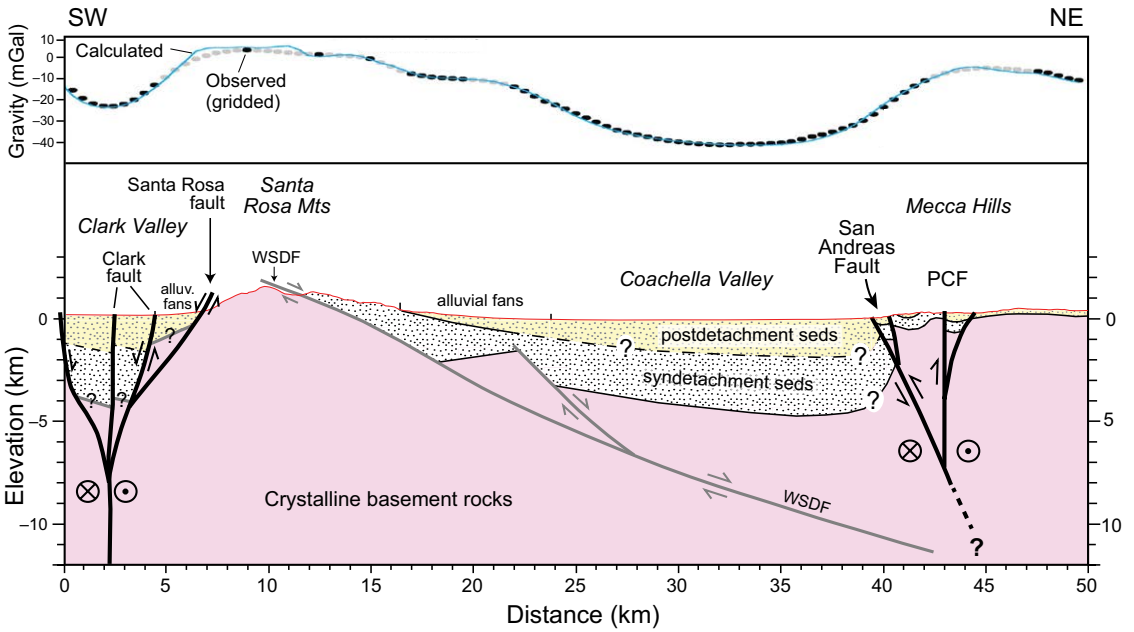

Figure 10. Gravity profile and interpreted geologic cross section across the southern Coachella Valley and Santa Rosa Mountains (see Fig. 1 for location). Gravity data were gridded using the minimum curvature algorithm of Briggs (1974); gravity points are gray where the grid was constrained by measurements more than 2–3 km from the profile. Basement surface is based on two-dimensional forward modeling of the gravity data, which reveal a 3–4-km-deep fault-bounded basin beneath Clark Valley and northeastward thickening of sediment beneath the southern Coachella Valley to an abrupt boundary at the San Andreas fault. WSDF—West Salton detachment fault; PCF—Painted Canyon fault; alluv.—alluvial.

Geosphere, published online on 27 August 2015 as doi:10.1130/GES01167.1

We infer similar extension in this area. A step in the gravity profile suggests the presence of a steep normal fault and large basement rider block buried beneath sediment in the upper plate of the WSDF. The lack of surface expression of this fault suggests that it is not currently active or has a very slow slip rate.

In addition to dextral offset of ~17 km on the Clark fault (Janecke et al., 2010), map relations in the southern Santa Rosa Mountains and the large gravity low in Clark Valley suggest significant vertical displacement on splaying fault strands in Clark Valley (Figs. 3 and 10). The WSDF in the Santa Rosa Mountains projects to a height of ~2–2.5 km above Clark Lake. Adding this to the depth of the detachment fault inferred beneath Clark Valley (3–4 km) indicates ~5.0–6.5 km of combined vertical separation across the Santa Rosa and Clark faults (Fig. 10). The true vertical offset could be, and likely is, considerably less than this if structural markers that started at different elevations have been juxtaposed by strike-slip motion. A conservative estimate of vertical offset is obtained by adding the height of the highest triangular facets on the Santa Rosa fault (~0.6 km), the drop in elevation down steep alluvial fans from the fault trace to the valley floor (~0.3 km), and the thickness of postdetachment sediments in the subsurface which is not known. Because Clark Valley has been an actively subsiding transtensional depocenter for the past ~1.2 m.y. (Lutz et al., 2006), we infer that postdetachment sediments are at least 0.5–1.0 km thick in Clark Valley, suggesting combined vertical displacement of at least 1.5–2.0 km across the Santa Rosa and Clark faults.

Subsurface sediment in the southern Coachella Valley thickens gradually to the northeast from a tapered edge on the southwest side of Coachella Valley to a depth of ~5 km, where it is abruptly truncated at the SAF (Fig. 10). Although the depth to the contact between syndetachment and postdetachment sediments is not known, we infer that postdetachment deposits thicken to the northeast across the southern Coachella Valley based on the presence of northeastward-fanning dips in the upper 2–3 km of sediment beneath the northern Salton Sea (Fig. 1, Line 7; Kell et al., 2012; Fuis et al., 2012b, 2012c; see following discussion). A steep northeast dip on the SAF is suggested by seismic, magnetic, geodetic, and modeling studies (Lin et al., 2007; Fuis et al., 2012a; Langenheim et al., 2012; Lindsey and Fialko, 2013; Fattaruso et al., 2014) and is used in our cross section (Fig. 10).

DISCUSSION

Summary of Observations

This study documents new geomorphic, geologic, and geophysical evidence for active northeastward tilting of the Santa Rosa Mountains and southern Coachella Valley between the San Jacinto and San Andreas faults (Fig. 1). Data that support crustal-scale northeast tilting include: (1) asymmetric crustal structure with large vertical offsets on the San Jacinto fault and SAF zones (Fig. 10); (2) contrasting morphology across the Santa Rosa Mountains, with a steep active faulted range front on the southwest and large low-gradient, unfaulted alluvial fans on the northeast (Figs. 4–6 and 8); (3) geologic evidence for substantial postdetachment uplift in the footwall of the Santa Rosa fault (Fig. 3); (4) the presence of tilted and incised late Pleistocene alluvial fans in the northeast Santa Rosa Mountains (Fig. 7); (5) lower ratios of fan area to catchment area (Af/Ac) on the southwest side of the range and higher ratios on the northeast (Fig. 9); and (6) northeastward thickening of sediment beneath the Coachella Valley to an abrupt margin at the SAF (Figs. 1, 2, and 10). The proposed tilt direction is consistent with a receiver function study showing that the base of the crust is deeper southwest of the San Jacinto fault and shallower northeast of the San Jacinto fault (Miller et al., 2014).

The depth to the contact between syndetachment and postdetachment sediments beneath the southern Coachella Valley is not known due to a lack of seismic reflection data and deep wells in the valley. However, late Quaternary to Holocene postdetachment fan deposits overlie syndetachment deposits along a northeast-dipping unconformity at the irregular eastern edge of the eastern Santa Rosa Mountains (Fig. 3). This contact projects northeast into the subsurface of the southern Coachella Valley, and is present at unknown depth where the total sediment thickness is 4–5 km close to the SAF (Fig. 10). If the accumulation rate is similar to that documented nearby in rapidly subsiding depocenters of the Salton Trough (1–2 mm/yr; Herzig et al., 1988; Schmitt and Hulen, 2008; Dorsey et al., 2011; McNabb, 2013), we would predict a depth of ~1.2–2.4 km to the contact between predetachment and postdetachment deposits in the subsurface. Combining the asymmetric morphology of the Santa Rosa Mountains, wedge-shaped basin geometry beneath the southern Coachella Valley, and possible range of depth to the base of postdetachment deposits (Fig. 10), we estimate that the central Salton block has tilted ~5°–10° to the northeast since ca. 1.2 Ma (age of the SJFZ).

Although our estimate of northeast tilting is hindered by limited subsurface data, a similar geometry and amount of tilting was documented in a recent seismic-reflection study of the northern Salton Sea (L-7 in Fig. 1), where sediments in the upper 3–4 km display northeastward-fanning dips toward the SAF at dip values to ~8° (Kell et al., 2012; Fuis et al., 2012b, 2012c). In the southern Salton Sea, the presence of the 770 ka Bishop ash interbedded with lake deposits at a depth of 1.7 km and 430 ka extrusive rhyolites buried to depths of 2 km nearby record subsidence and accumulation at a rate of ~2–4 mm/yr (Herzig et al., 1988; Schmitt and Hulen, 2008). At these rates, fanning dips in the upper 3–4 km of sediment in line 7 (Kell et al., 2012; Fuis et al., 2012b, 2012c) record tilting over the past ~1–2 m.y. Systematic northeast dips of 5°–10° in subsurface sediments are also imaged in a nearby seismic reflection study of the San Felipe Badlands southwest of the Salton Sea (S in Fig. 1; Severson, 1987). Thus, while it is difficult to quantify the amount of postdetachment tilt, our conclusion of ~5°–10° in the past ~1.2 m.y. is supported by young sediments beneath the northern Salton Sea that display a style, scale, geometry, and timing of northeast tilting that are strikingly similar to the tilt geometry and timing estimated in this study for the Santa Rosa Mountains and southern Coachella Valley.

Geosphere, published online on 27 August 2015 as doi:10.1130/GES01167.1

Spatial Extent of Crustal Tilting

The lateral extent of the crustal block involved in northeastward tilting can be inferred from regional geology, geomorphology, and gravity. Gravity data reveal an along-strike change from a northeast-dipping basin floor in the southeast Coachella Valley to a shallower irregular basin geometry in the northwestern Coachella Valley (Fig. 1). This change coincides with a prominent northeast-trending ridge that protrudes northeast into the Coachella Valley across from the junction of the Banning and Mission Creek faults (Ridge in Fig. 2). These features suggest the presence of a structural boundary between a more intact, northeast-tilted crustal block in the southern Coachella Valley and a segmented crustal structure in the northern Coachella Valley (Fig. 1). North of this boundary, the San Jacinto Mountains lack the pronounced asymmetric morphology seen in the Santa Rosa Mountains, suggesting the possible absence of northeast tilting in the San Jacinto Mountains and northern Coachella Valley. The implied structural boundary may be controlled by a poorly understood tear fault at the northwestern boundary of a relatively intact northeast-dipping tilt block.

Structural disruption and segmentation are also evident southeast of the Santa Rosa Mountains in a zone of intense active transpressional deformation related to active dextral faulting and rotation in the SJFZ (Brothers et al., 2009; Janecke et al., 2010; Thornock, 2013). Extreme structural complexity in this area is related to interaction of the Clark and Extra fault zones, and may reflect ongoing breakup of a corner of the Salton block due to the local effects of clockwise crustal rotation. Despite these complexities, seismic reflection studies provide evidence for systematic northeastward tilting in the subsurface of the central to northern Salton Sea and adjacent parts of the western Salton Trough (Fig. 1; Severson, 1987; Kell et al., 2012; Fuis et al., 2012b, 2012c). The distribution of faults suggests that the zone of northeastward crustal tilting may continue southeast to the Extra fault zone in the Salton Sea (Brothers et al., 2009); if so, the northeast-tilting fault block would be ~35 km wide and 50–60 km long, with significant structural complexity and disruption in the southeast.

Controls on Crustal Tilting

We consider several processes that could drive northeastward tilting of an ~35-km-wide crustal block between the San Jacinto and San Andreas faults about a horizontal axis during the past ~1.2 m.y.: (1) oblique convergence and loading across a northeast-dipping SAF in Coachella Valley; (2) dextral translation of crust through a releasing bend in the Santa Rosa fault; (3) vertical loading by mafic intrusions beneath the southern Salton Sea; and (4) short-wavelength upper mantle convection related to lithospheric drips or delamination.

1. Although the southern SAF in Coachella Valley is widely considered to be vertical (e.g., Meade and Hager, 2005; Loveless and Meade, 2011; Herbert and Cooke, 2012; Luo and Liu, 2012; Nicholson et al., 2013), recent seismic, geophysical, and modeling studies suggest that it dips steeply northeast (Lin et al., 2007; Fuis et al., 2012a; Lindsey and Fialko, 2013; Fattaruso et al., 2014). A small component of convergence across a northeast-dipping SAF can produce a vertical load that may drive northeast tilting of the Salton block (Fig. 11). GPS data appear to support this hypothesis. The SAF in the Coachella Valley strikes N46°W (Fig. 1). An average of GPS-based Pacific–North America plate motions calculated from 8 studies in California is 49 mm/yr toward N38°W (DeMets et al., 2010). GPS sites on the Salton block show that it is moving along an azimuth of N37°W and N43°W relative to stable North America, with an average direction of N40°W at rates varying from ~10 to 23 mm/yr (Spinler et al., 2010). The average motion of the Salton block relative to North America thus is oriented ~6°–8° clockwise from the strike of the SAF in Coachella Valley, suggesting a small component of convergence across the Coachella Valley strand of the SAF (Fig. 11). This inference is supported by geologic structures in the Mecca Hills, northeast of the SAF in the southern Coachella Valley, that record active transpression and shortening adjacent to the SAF in this area (Fig. 1; Sylvester and Smith, 1976, 1987; Rymer, 1991, 1994; Sheridan and Weldon, 1994; McNabb, 2013).

The 3-D boundary element models show that a small angle of convergence across a northeast-dipping SAF produces significant northeast tilting that includes subsidence in the Coachella Valley and uplift in the Santa Rosa Mountains (Fattaruso et al., 2014). The pattern of progressive tilting predicted by the model agrees closely with the pattern of northeast tilting documented in this study (Fig. 10); models that assume a vertical southern SAF do not replicate the observed tilt pattern (Fattaruso et al., 2014). According to this hypothesis, uplift of the Santa Rosa Mountains results from (1) vertical loading at the northeast side of the Salton block as a result of oblique convergence across the SAF;

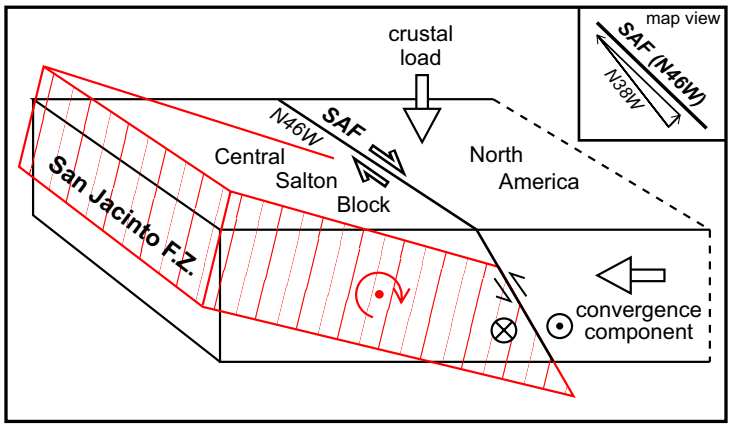

Figure 11. Conceptual diagram illustrating hypothesis for northeastward tilting of the central Salton block in response to oblique shortening across steeply northeast-dipping San Andreas fault (SAF) in Coachella Valley. Inset is a slip vector diagram showing the small angle of oblique convergence across the southern SAF (Fattaruso et al., 2014). Rates of strike-slip motion in this area vary along strike from ~14 to 23 mm/yr (Spinler et al., 2010; Behr et al., 2010). F.Z.—fault zone.

Geosphere, published online on 27 August 2015 as doi:10.1130/GES01167.1

(2) conservation of mass: as the northeast side is displaced downward, the rest of the block must also be displaced; (3) force imbalance due to the presence of a downward load in the northeast and absence of a similar load in the southwest; (4) uniform crustal buoyancy, and (5) subvertical SJFZ, which provides a break in the crust to accommodate vertical displacement (Fig. 11). The crust responds by rigid tilting across the full width of the Salton block because the effective elastic thickness in this area is ~15 km (Fay and Humphreys, 2005). This corresponds to a flexural wavelength of at least 60–80 km, much greater than the across-strike width of the Salton block (30–35 km).

As the Salton block tilts, the faults bounding it may also tilt through time in a manner analogous to progressive rotation of normal faults in extended terranes (e.g., Jackson and McKenzie, 1983; Sharp et al., 2000). This would imply that the SAF originally had a shallower northeast dip, and the SJFZ may have started with a steep northeast dip. Alternatively, block tilting may occur without significant reorientation of bounding faults if the fault zones can crush and redistribute a sufficient volume of rock through time. Rotation of the faults, if active, likely is a minor effect since the total amount of tilting is <10°.

2. Crustal tilting in strike-slip fault zones may occur as a response to torques applied by translation of crust through large bends in a master strike-slip fault (e.g., Mann, 1997; Aksu et al., 2000; Cormier et al., 2006; Sorichetta et al., 2010). The discontinuity between the southern and northern Coachella Valley and lack of evidence for tilting in the San Jacinto Mountains suggest that northeast tilting in the Santa Rosa Mountains and southern Coachella Valley is not directly related to translation through the large restraining bend in San Gorgonio Pass (Fig. 1). However, if the northwest-trending northwest segment of the Santa Rosa fault has significant dextral slip, as suggested by the preponderance of northwest-striking dextral faults in the SJFZ (Fig. 1), a releasing bend would be inferred where the fault strike changes from northwest in the north to north-northwest in the south (Fig. 3). Translation through this releasing bend could drive footwall uplift in the southern Santa Rosa Mountains and contribute to partitioning of transtensional strain on neighboring strike-slip and normal faults. While this mechanism is plausible, we consider it unlikely because there is no known evidence for major dextral offset on the northwest segment of the Santa Rosa fault, and the scale and angle of the implied releasing bend are small relative to the Salton block.

3. Dense mafic intrusions are another possible driver of subsidence. Buried basaltic intrusive bodies are indicated by the presence of a large gravity high in the southern Salton Sea (Fig. 2) in the middle of the deep sediment-filled Salton Trough basin (e.g., Fuis et al., 1984; Herzig et al., 1988; Han et al., 2013). However, the center of the gravity high is located slightly east of the Brawley seismic zone (Fig. 2), indicating that the main intrusion is not today entirely in the Salton block. Brothers et al. (2009) suggested that the releasing stepover geometry of the modern Brawley seismic zone may have initiated as recently as ca. 0.5 Ma, and prior to that time the main SAF continued to the southeast along the northeast margin of the Salton Trough. If correct, this would imply that the mafic intrusions were within the Salton block until the inferred reorganization ca. 0.5 Ma. Nonetheless, high heat flow should weaken the crust around intrusions and limit the effects of loading to a small area. Thus we conclude that vertical loading by mafic intrusions beneath the southern Salton Sea probably does not play a major role in northeastward crustal tilting documented in this study.

4. Vertical foundering of a dense eclogitic root into the upper mantle has been inferred as the driving force for uplift and tilting in the Sierra Nevada Mountains (Zandt et al., 2004; Boyd et al., 2004; Saleeby and Foster, 2004; Maheo et al., 2009) and Wallowa Mountains in Oregon (Hales et al., 2005). Numerical models show that vertical drips of dense lithospheric bodies can produce Rayleigh-Taylor instabilities that generate vertical motions of the crust and Earth's surface at a wide range of spatial scales, including the length scale of tilting documented here (Le Pourhiet et al., 2006; Gogus and Pysklywec, 2008; Harig et al., 2008). Receiver function studies show that high topography of the eastern Peninsular Ranges lacks an Airy crustal root and is supported by upper mantle buoyancy (Lewis et al., 2000, 2001; Persaud et al., 2007). The geometry, distribution, and post-Pliocene timing of uplift in the Peninsular Ranges suggest that removal of mantle lithosphere is related to the modern phase of transform tectonics (Mueller et al., 2009). Numerical modeling based on surface-wave tomography shows that small-scale upper mantle convection plays an important role in driving transpressional crustal deformation in the Transverse Ranges (Fay et al., 2008). If loading from below were applied unevenly, it could produce tilting geometries difficult to predict in detail. Thus we consider short-wavelength upper mantle convection to be a plausible but untested control on tilting of the Salton block.

CONCLUSIONS

Geologic, geomorphic, and geophysical data indicate that the central Salton block is undergoing systematic northeastward tilting between the San Jacinto and San Andreas faults. This conclusion is supported by (1) geologic and gravity evidence for large vertical offsets on the San Jacinto and SAF zones; (2) a steep fault-controlled range front at the southwest margin of the southern Santa Rosa Mountains and large low-gradient alluvial fans on the northeast side; (3) lower ratios of fan area to catchment area (Af/Ac) in the southwest Santa Rosa Mountains compared to higher ratios on the northeast side; (4) evidence for substantial postdetachment uplift in the footwall of the Santa Rosa fault; (5) the presence of tilted and incised late Pleistocene alluvial fans in the northeast Santa Rosa Mountains; and (6) progressive northeastward thickening of sediment beneath the Coachella Valley to an abrupt margin at the SAF (Figs. 1 and 10). Northeastward tilting likely began ca. 1.2 Ma when a regional tectonic reorganization initiated the SJFZ.

Processes that may drive crustal tilting include (1) oblique convergence and vertical loading across a northeast-dipping SAF in Coachella Valley; (2) dextral translation of crust through a hypothesized releasing bend in the Santa Rosa fault; (3) loading by buried mafic intrusions beneath the southern Salton Sea; and (4) short-wavelength upper mantle convection. Hypothesis 1, oblique

Geosphere, published online on 27 August 2015 as doi:10.1130/GES01167.1

convergence across a northeast-dipping San Andreas fault, is supported by a recent boundary-element modeling study (Fattaruso et al., 2014) and appears to be a likely driver of crustal tilting. We consider hypotheses 2 and 3 to be unlikely, and suggest hypothesis 4 as a plausible but as-yet untested control on active tilting of the central Salton block.

ACKNOWLEDGMENTS

Support for this study was provided by National Science Foundation grant EAR-1144946 (Dorsey), and by the National Cooperative Geologic Mapping and Earthquake Hazards programs of the U.S. Geological Survey (Langenheim). This study benefited from discussions with Michele Cooke, Laura Fattaruso, Cody Mason, and Charlie Ogle. Reviews by Robert Powell, Keith Howard, Nathan Niemi, Andy Barth, Terry Pavlis, Francesco Mazzarini, and three anonymous reviewers helped us improve the quality and clarity of the paper.

REFERENCES CITED

Aksu, A.E., Colon, T.J., Hiscott, R.N., and Yasar, D., 2000, Anatomy of the North Anatolian fault zone in the Marmara Sea, western Turkey: Extensional basins above a continental transform: GSA Today, v. 10, p. 3–7.

Allen, C.R., 1957, San Andreas fault zone in the San Gorgonio Pass, southern California: Geological Society of America Bulletin, v. 68, p. 315–350, doi:10.1130/0016-7606(1957)68[315:SAFZIS]2.0.CO;2.

Allen, P.A., and Densmore, A.L., 2000, Sediment flux from an uplifting fault block: Basin Research, v. 12, p. 367–380, doi:10.1046/j.1365-2117.2000.00135.x.

Allen, P.A., and Hovius, N., 1998, Sediment supply from landslide-dominated catchments: Implications for basin-margin fans: Basin Research, v. 10, p. 19–35, doi:10.1046/j.1365-2117.1998.00060.x.

Axen, G.J., and Fletcher, J.M., 1998, Late Miocene–Pleistocene extensional faulting, northern Gulf of California, Mexico and Salton Trough, California: International Geology Review, v. 40, p. 217–244, doi:10.1080/00206819809465207.

Bartholomew, M.J., 1970, San Jacinto fault zone in the northern Imperial Valley, California: Geological Society of America Bulletin, v. 81, p. 3161–3166, doi:10.1130/0016-7606(1970)81[3161:SJFZIT]2.0.CO;2.

Behr, W.M., et al., 2010, Uncertainties in slip rate estimates for the Mission Creek strand of the southern San Andreas fault at Biskra Palms Oasis, southern California: Geological Society of America Bulletin, v. 122, p. 1360–1377, doi:10.1130/B30020.1.

Belgarde, B.E., 2007, Structural characterization of the three southeast segments of the Clark fault, Salton Trough, California [M.S thesis]: Logan, Utah State University, 216 p.

Ben-Avraham, Z., and Zoback, M.D., 1992, Transform-normal extension and asymmetric basins: An alternative to pull-apart models: Geology, v. 20, p. 423–426, doi:10.1130/0091-7613(1992)020<0423:TNEAAB>2.3.CO;2.

Bennett, R., Rodi, W., and Reilinger, R., 1996, Global positioning system constraints on fault slip rates in southern California and northern Baja, Mexico: Journal of Geophysical Research, v. 101, no. B10, p. 21,943–21,960, doi:10.1029/96JB02488.

Bennett, R.A., Friedrich, A.M., and Furlong, K.P., 2004, Codependent histories of the San Andreas and San Jacinto fault zones from inversion of fault displacement rates: Geology, v. 32, p. 961–964, doi:10.1130/G20806.1.

Biehler, S., Langenheim, V.E., Sikora, R.F., Chapman, R.H., and Beyer, L.A., 1992, Complete Bouguer gravity anomaly map of the Santa Ana 1 degree by 2 degrees quadrangle, California: U.S. Geological Survey Open-File Report 92-279.

Blisniuk, K., Rockwell, T., Owen, L.A., Oskin, M., Lippincott, C., Caffee, M.W., and Dortch, J., 2010, Late Quaternary slip rate gradient defined using high-resolution topography and ^{10}Be dating of offset landforms on the southern San Jacinto fault zone, California: Journal of Geophysical Research, v. 115, B08401, doi:10.1029/2009JB006346.

Bortugno, E.J., and Spittler, T.E., 1986, Geologic map of the San Bernardino quadrangle: California Division of Mines and Geology Regional Geologic Map Series no. 3A, scale 1:250,000.

Boyd, O.S., Jones, C.H., and Sheehan, A.F., 2004, Foundering lithosphere imaged beneath the southern Sierra Nevada, California, USA: Science, v. 305, p. 660–662, doi:10.1126/science.1099181.

Briggs, I.C., 1974, Machine contouring using minimum curvature: Geophysics, v. 39, p. 39–48, doi:10.1190/1.1440410.

Brothers, D.S., Driscoll, N.W., Kent, G.M., Harding, A.J., Babcock, J.M., and Baskin, R.L., 2009, Tectonic evolution of the Salton Sea inferred from seismic reflection data: Nature Geoscience, v. 2, p. 581–584, doi:10.1038/ngeo590.

Carena, S., Suppe, J., and Kao, H., 2004, Lack of continuity of the San Andreas fault in southern California: Three-dimensional fault models and earthquake scenarios: Journal of Geophysical Research, v. 109, B04313, doi:10.1029/2003JB002643.

Cooke, M., and Dair, L., 2011, Simulating the recent evolution of the southern big bend of the San Andreas fault, southern California: Journal of Geophysical Research, v. 116, B04405, doi:10.1029/2010JB007835.

Cooke, M.L., Schottenfelf, M.T., and Buchanan, S.W., 2013, Evolution of fault efficiency at restraining bends within wet kaolin analog experiments: Journal of Structural Geology, v. 51, p. 180–192, doi:10.1016/j.jsg.2013.01.010.

Cormier, M.H., et al., 2006, The North Anatolian fault in the Gulf of Izmit (Turkey): Rapid vertical motion in response to minor bends of a non-vertical continental transform: Journal of Geophysical Research, v. 111, B04102, doi:10.1029/2005JB003633.

Cox, B.F., Matti, J.C., King, T., and Morton, D.M., 2002, Neogene strata of southern Santa Rosa Mountains, California, and their significance for tectonic evolution of the western Salton Trough: Geological Society of America Abstracts with Programs, v. 34, no. 6, paper 57–5.

Crowell, J.C., 1974, Origin of late Cenozoic basins in southern California, *in* Dickinson, W.R., ed., Tectonics and sedimentation: Society of Economic Paleontologists and Mineralogists Special Publication 22, p. 190–204, doi:10.2110/pec.74.22.0190.

Crowell, J.C., 1981, An outline of the tectonic history of southeastern California, *in* Ernst, W.G., ed., The geotectonic development of California; Rubey Volume I: Englewood Cliffs, New Jersey, Prentice-Hall, p. 583–600.

Dade, W.B., and Verdeyen, M.E., 2007, Tectonic and climatic controls of alluvial-fan size and source-catchment relief: Geological Society of London Journal, v. 164, p. 353–358, doi:10.1144/0016-76492006-039.

Dair, L., and Cooke, M., 2009, San Andreas fault geometry through the San Gorgonio Pass, California: Geology, v. 37, p. 119–122, doi:10.1130/G25101A.1.

Darin, M.H., and Dorsey, R.J., 2013, Reconciling disparate estimates of total offset on the southern San Andreas fault: Geology, v. 41, p. 975–978, doi:10.1130/G34276.1.

DeMets, C., Gordon, R.G., and Argus, D.F., 2010, Geologically current plate motions: Geophysical Journal International, v. 181, p. 1–80, doi:10.1111/j.1365-246X.2009.04491.x.

dePolo, C.M., and Anderson, J.G., 2000, Estimating the slip rates of normal faults in the Great Basin, USA: Basin Research, v. 12, p. 227–240, doi:10.1046/j.1365-2117.2000.00131.x.

Dibblee, T.W., Jr., 1954, Geology of the Imperial Valley region, California, *in* Jahns, R.H., ed., Geology of southern California: California Division of Mines Bulletin 170, p. 21–28.

Dibblee, T.W., 1984, Stratigraphy and tectonics of the San Felipe Hills, Borrego Badlands, Superstition Hills, and vicinity, *in* Rigsby, C.A., ed., The Imperial Basin—Tectonics, sedimentation, and thermal aspects: Los Angeles, California, Pacific Section, Society of Economic Paleontologists and Mineralogists, p. 31–44.

Dibblee, T.W., 2008, Geologic map of the Clark Lake & Rabbit Peak 15 minute quadrangles, Riverside, San Diego, and Imperial Counties, California: Santa Barbara, California, Santa Barbara Museum of Natural History, scale 1:62,500.

Dorsey, R.J., 2002, Stratigraphic record of Pleistocene initiation and slip on the Coyote Creek fault, lower Coyote Creek, southern California, *in* Barth, A., ed., Contributions to crustal evolution of the southwest United States: Geological Society of America Special Paper 365, p. 251–269, doi:10.1130/0-8137-2365-5.251.

Dorsey, R.J., 2010, Sedimentation and crustal recycling along an active oblique-rift margin: Salton Trough and northern Gulf of California: Geology, v. 38, p. 443–446, doi:10.1130/G30698.1.

Dorsey, R.J., Fluette, A., McDougall, K.A., Housen, B.A., Janecke, S.U., Axen, G.J., and Shirvell, C.R., 2007, Chronology of Miocene–Pliocene deposits at Split Mountain Gorge, southern California: A record of regional tectonics and Colorado River evolution: Geology, v. 35, p. 57–60, doi:10.1130/G23139A.1.

Dorsey, R.J., Housen, B.A., Janecke, S.U., Fanning, C.M., and Spears, A.L.F., 2011, Stratigraphic record of basin development within the San Andreas fault system: Late Cenozoic Fish

Geosphere, published online on 27 August 2015 as doi:10.1130/GES01167.1

Creek–Vallecito basin, southern California: Geological Society of America Bulletin, v. 123, p. 771–793, doi:10.1130/B30168.1.

Dorsey, R.J., Axen, G.J., Peryam, T.C., and Kairouz, M.E., 2012, Initiation of the southern Elsinore fault at ~1.2 Ma: Evidence from the Fish Creek–Vallecito Basin, southern California: Tectonics, v. 31, TC2006, doi:10.1029/2011TC003009.

Ehlig, P.L., 1981, Origin and tectonic history of the basement terrane of the San Gabriel Mountains, central Transverse Ranges, *in* Ernst, W.G., ed., The geotectonic development of California; Rubey Volume I: Englewood Cliffs, New Jersey, Prentice-Hall, p. 253–283.

Elders, W.A., and Sass, J.H., 1988, The Salton Sea scientific drilling project: Journal of Geophysical Research, v. 93, no. B11, p. 12,953–12,968, doi:10.1029/JB093iB11p12953.

Fattaruso, L., Cooke, M.L., and Dorsey, R.J., 2014, Sensitivity of uplift patterns to dip of the San Andreas fault in the Coachella Valley, CA: Geosphere, v. 10, p. 1235–1246, doi:10.1130/GES01050.1.

Fay, N., and Humphreys, E., 2005, Fault slip rates, effects of elastic heterogeneity on geodetic data, and the strength of the lower crust in the Salton Trough region, southern California: Journal of Geophysical Research, v. 110, B09401, doi:10.1029/2004JB003548.

Fay, N., and Humphreys, E., 2006, Dynamics of the Salton block: Absolute fault strength and crust-mantle coupling in southern California: Geology, v. 34, p. 261–264, doi:10.1130/G22172.1.

Fay, N., Bennett, R.A., Spinler, J.C., and Humphreys, E.D., 2008, Small-scale upper mantle convection and crustal dynamics in southern California: Geochemistry, Geophysics, Geosystems, v. 9, Q08006, doi:10.1029/2008GC001988.

Fuis, G.S., Mooney, W.D., Healy, J.H., McMechan, G.A., and Lutter, W.J., 1984, A seismic refraction survey of the Imperial Valley region, California: Journal of Geophysical Research, v. 89, p. 1165–1189, doi:10.1029/JB089iB02p01165.

Fuis, G.S., Scheirer, D.S., Langenheim, V.E., and Kohler, M.D., 2012a, A new perspective on the geometry of the San Andreas fault in southern California and its relationship to lithospheric structure: Seismological Society of America Bulletin, v. 102, p. 236–251, doi:10.1785/0120110041.

Fuis, G., et al., 2012b, Investigating earthquake hazards in the northern Salton Trough, southern California, using data from the Salton Seismic Imaging Project (SSIP): American Geophysical Union Fall Meeting 2012, abs. T44A-06.

Fuis, G., et al., 2012c, Investigating earthquake hazards in the northern Salton Trough, southern California, using data from the Salton Seismic Imaging Project (SSIP) [poster]: U.S. Geological Survey Earthquake Hazards Program, Salton Seismic Imaging Project, http://earthquake.usgs.gov/research/salton/SSIP-poster-2012-12.pdf

Gawthorpe, R.L., and Leeder, M.R., 2000, Tectono-sedimentary evolution of active extensional basins: Basin Research, v. 12, p. 195–218, doi:10.1046/j.1365-2117.2000.00121.x.

Gogus, O.H., and Pysklywec, R.N., 2008, Near-surface diagnostics of dripping or delaminating lithosphere: Journal of Geophysical Research, v. 113, B11404, doi:10.1029/2007JB005123.

Gray, H.J., Owen, L.A., Dietsch, C., Beck, R.A., Caffee, M.A., Finkel, R.C., and Mahan, S.A., 2014, Quaternary landscape development, alluvial fan chronology and erosion of the Mecca Hills at the southern end of the San Andreas fault zone: Quaternary Science Reviews, v. 105, p. 66–85, doi:10.1016/j.quascirev.2014.09.009.

Gueguen, E., Tavarnelli, E., Renda, P., and Tramutoli, M., 2010, The southern Tyrrhenian Sea margin: An example of lithospheric scale strike-slip duplex: Italian Journal of Geosciences, v. 129, p. 496–505, doi:10.3301/IJG.2010.15.

Hales, T.C., Abt, D.L., Humphreys, E.D., and Roering, J.J., 2005, A lithospheric instability origin for Columbia River flood basalts and Wallowa Mountains uplift in northeast Oregon: Nature, v. 438, p. 842–845, doi:10.1038/nature04313.

Han, L., Hole, J.A., Stock, J.M., Fuis, G.S., Driscoll, N.W., Kell, A.M., Kent, G., Harding, A.J., and Gonzalez-Fernandez, O.L., 2013, Crustal structure during active rifting in the central Salton Trough, California, constrained by the Salton Seismic Imaging Project (SSIP): American Geophysical Union Fall Meeting 2013, abs. T11D-2478.

Harden, J., and Matti, J., 1989, Holocene and late Pleistocene slip rates on the San Andreas fault in Yucaipa, California, using displaced alluvial-fan deposits and soil chronology: Geological Society of America Bulletin, v. 101, p. 1107–1117, doi:10.1130/0016-7606(1989)101<1107:HALPSR>2.3.CO;2.

Harig, C., Molnar, P., and Houseman, G.A., 2008, Rayleigh-Taylor instability under a shear stress free top boundary condition and its relevance to removal of mantle lithosphere from beneath the Sierra Nevada: Tectonics, v. 27, TC6019, doi:10.1029/2007TC002241.

Herbert, J.W., and Cooke, M.L., 2012, Sensitivity of the Southern San Andreas fault system to tectonic boundary conditions and fault configurations: Seismological Society of America Bulletin, v. 102, p. 2046–2062, doi:10.1785/0120110316.

Herzig, C.T., Mehegan, J.M., and Stelting, C.E., 1988, Lithostratigraphy of the State 2–14 Borehole; Salton Sea Scientific Drilling Project: Journal of Geophysical Research, v. 93, p. 12,969–12,980, doi:10.1029/JB093iB11p12969.

Hooke, R.L., 1972, Geomorphic evidence for late Wisconsin and Holocene tectonic deformation in Death Valley, California: Geological Society of America Bulletin, v. 83, p. 2073–2098, doi:10.1130/0016-7606(1972)83[2073:GEFLAH]2.0.CO;2.

Jachens, R.C., and Moring, B.C., 1990, Maps of the thickness of Cenozoic deposits and the isostatic residual gravity over basement for Nevada: U.S. Geological Survey Open-File Report 90–404, 15 p.

Jackson, J., and McKenzie, D., 1983, The geometrical evolution of normal fault systems: Journal of Structural Geology, v. 5, p. 471–482, doi:10.1016/0191-8141(83)90053-6.

Janecke, S.U., Dorsey, R.J., Steely, A.N., Kirby, S.M., Lutz, A.T., Housen, B.A., Belgarde, B., Langenheim, V., Rittenour, T., and Forand, D., 2010, High geologic slip rates since early Pleistocene initiation of the San Jacinto and San Felipe fault zones in the San Andreas fault system: Southern California, USA: Geological Society of America Special Paper 475, 48 p., doi:10.1130/9780813724751.

Jennings, C.W., compiler, 1977, Geologic map of California: California Division of Mines and Geology Geologic Data Map 2, scale 1:750,000.

Kasameyer, P.W., and Hearst, J.R., 1988, Borehole gravity measurements in the Salton Sea Scientific Drilling Project Well State 2–14: Journal of Geophysical Research, v. 93, no. B11, p. 13,037–13,045, doi:10.1029/JB093iB11p13037.

Kell, A.M., Sahakian, V.J., Harding, A.J., Kent, G., and Driscoll, N.W., 2012, Shallow sediment and upper crustal structure beneath the Salton Sea as imaged by active source marine seismic refraction in conjunction with the Salton Seismic Imaging Project: American Geophysical Union Fall Meeting 2012, abs. T51B-2578.

Keller, E.A., Bonkowski, M.S., Korsch, R.J., and Shlemon, R.J., 1982, Tectonic geomorphology of the San Andreas fault zone in the southern Indio Hills, Coachella Valley, California: Geological Society of America Bulletin, v. 93, p. 46–56, doi:10.1130/0016-7606(1982)93<46:TGOTSA>2.0.CO;2.

King, T., Cox, B.F., Matti, J.C., Powell, C.L., Osterman, L.E., and Bybell, L.M., 2002, Previously unreported outcrops of Neogene Imperial Formation in southern Santa Rosa Mountains, California, and implications for tectonic uplift: Geological Society of America Abstracts with Programs, v. 34, no. 6., paper 57-6.

Kirby, S.M., Janecke, S.U., Dorsey, R.J., Housen, B.A., Langenheim, V., McDougall, K., and Steely, A.N., 2007, Pleistocene Brawley and Ocotillo formations: Evidence for initial strike-slip deformation along the San Felipe and San Jacinto fault zones, southern California: Journal of Geology, v. 115, p. 43–62, doi:10.1086/509248.

Langenheim, V.E., Jachens, R.C., Morton, D.M., Kistler, R.W., and Matti, J.C., 2004, Geophysical and isotopic mapping of pre-existing crustal structures that influenced the location and development of the San Jacinto fault zone, southern California: Geological Society of America Bulletin, v. 116, p. 1143–1157, doi:10.1130/B25277.1.

Langenheim, V.E., Jachens, R.C., Matti, J.C., Hauksson, E., and Christensen, A., 2005, Geophysical evidence for wedging in the San Gorgonio Pass structural knot, southern San Andreas fault zone, southern California: Geological Society of America Bulletin, v. 117, p. 1554–1572, doi:10.1130/B25760.1.

Langenheim, V.E., Biehler, S., McPhee, D.K., McCabe, C.A., Watt, J.T., Anderson, M.L., Chuchel, B.A., and Stoffer, P., 2007, Preliminary isostatic gravity map of Joshua Tree National Park and vicinity, southern California: U.S. Geological Survey Open-File Report 2007-1218, scale 1:100,000.

Langenheim, V.E., Scheirer, D.S., Athens, N.D., and Fuis, G.S., 2012, Modeling of potential-field data along profiles of the Salton Sea Seismic Imaging Project transects, southern California: American Geophysical Union Fall Meeting 2012, abs. T44A-07.

Langenheim, V.E., Scheirer, D.S., Fuis, G., Goldman, M., Catchings, R., Ryberg, T., and Rymer, M.J., 2013, Comparison of potential-field and seismic-velocity structure along the Salton Sea Seismic Imaging Project transects, northern Salton Trough, southern California: Southern California Earthquake Center Annual Meeting Proceedings Volume XXIII, p. 123.

Le Pourhiet, L., Gurnis, M., and Saleeby, J., 2006, Mantle instability beneath the Sierra Nevada Mountains in California and Death Valley extension: Earth and Planetary Science Letters, v. 251, p. 104–119, doi:10.1016/j.epsl.2006.08.028.

Lewis, J.L., Day, S.M., Magistrale, H., Eakins, J., and Vernon, F., 2000, Regional crustal thickness variations of the Peninsular Ranges, southern California: Geology, v. 28, p. 303–306, doi:10.1130/0091-7613(2000)28<303:RCTVOT>2.0.CO;2.

Geosphere, published online on 27 August 2015 as doi:10.1130/GES01167.1

Lewis, J.L., Day, S.M., Magistrale, H., Castro, R.R., Astiz, L., Rebollar, C., Eakins, J., Vernon, F.L., and Brune, J.N., 2001, Crustal thickness of the Peninsular Ranges and Gulf extensional province in the Californias: Journal of Geophysical Research, v. 106, p. 13,599–13,611, doi:10.1029/2001JB000178.

Lin, G., 2013, Three-dimensional seismic velocity structure and precise earthquake relocations in the Salton Trough, southern California: Seismological Society of America Bulletin, v. 103, p. 2694–2708, doi:10.1785/0120120286.

Lin, G., Shearer, P.M., and Hauksson, E., 2007, Applying a three-dimensional velocity model, waveform cross-correlation, and cluster analysis to locate the southern California seismicity from 1981 to 2005: Journal of Geophysical Research, v. 112, B12309, doi:10.1029/2007JB004986.

Lindsey, E.O., and Fialko, Y., 2013, Geodetic slip rates in the southern San Andreas fault system: Effects of elastic heterogeneity and fault geometry: Journal of Geophysical Research, v. 118, p. 689–697, doi:10.1029/2012JB009358.

Loveless, J.P., and Meade, B.J., 2011, Stress modulation on the San Andreas fault by interseismic fault system interactions: Geology, v. 39, p. 1035–1038, doi:10.1130/G32215.1.

Luo, G., and Liu, M., 2012, Multi-timescale mechanical coupling between the San Jacinto fault and the San Andreas fault, southern California: Lithosphere, v. 4, p. 221–229, doi:10.1130/L180.1.

Lutz, A.T., Dorsey, R.J., Housen, B.A., and Janecke, S.U., 2006, Stratigraphic record of Pleistocene faulting and basin evolution in the Borrego Badlands, San Jacinto fault zone, southern California: Geological Society of America Bulletin, v. 118, p. 1377–1397, doi:10.1130/B25946.1.

Maheo, G., Saleeby, J., Saleeby, Z., and Farley, K.A., 2009, Tectonic control on southern Sierra Nevada topography, California: Tectonics, v. 28, TC6006, doi:10.1029/2008TC002340.

Mann, P., 1997, Model for the formation of large, transtensional basins in zones of tectonic escape: Geology, v. 25, p. 211–214, doi:10.1130/0091-7613(1997)025<0211:MFTFOL>2.3.CO;2.

Mann, P., 2007, Global catalogue, classification and tectonic origins of restraining and releasing bends on active and ancient strike- slip fault systems, *in* Cunningham, W.D., and Mann, P., eds., Tectonics of strike-slip restraining and releasing bends: Geological Society of London Special Publication 290, p. 13–142, doi:10.1144/SP290.2.

Martin, A.J., Nigbor, R.L., Pendergraft, D.M., and Steller, R.A., 1997, Geophysical characterization of the upper Borrego Valley, California, *in* Bell, R.S., compiler, Symposium on the application of geophysics to engineering and environmental problems: Reno, Nevada, Environmental and Engineering Society, SAGEEP 1997 Proceedings, v. II, p. 1011–1021.

Matti, J.C., and Morton, D.M., 1993, Paleogeographic evolution of the San Andreas fault in southern California: A reconstruction based on a new cross-fault correlation, *in* Powell, R.E., et al., eds., The San Andreas fault system: Displacement, palinspastic reconstruction, and geologic evolution: Geological Society of America Memoir 178, p. 107–159, doi:10.1130/MEM178-p107.

Matti, J.C., Morton, D.M., and Cox, B., 1985, Distribution and geologic relations of fault systems in the vicinity of the central Transverse Ranges, southern California: U.S. Geological Survey Open-File Report 85-365, scale 1:25,0000, 27 p.

Matti, J.C., Morton, D.M., and Cox, B., 1992, The San Andreas fault system in the vicinity of the central Transverse Ranges province, southern California: U.S. Geological Survey Open-File Report 92-354, 40 p.

Matti, J.C., Cox, B.F., Morton, D.M., Sharp, R.V., and King, T., 2002, Fault-bounded Neogene sedimentary deposits in the Santa Rosa Mountains, southern California: Crustal stretching or transpressional uplift?: Geological Society of America Abstracts with Programs, v. 34, no. 6, paper 57-4.

Matti, J.C., Morton, D.M., Cox, B.F., Landis, G.P., Langenheim, V.E., Premo, W.R., Kistler, R., Budahn, J.R., 2006, Fault-bounded late Neogene sedimentary deposits in the Santa Rosa Mountains, southern CA: Constraints on the Evolution of the San Jacinto fault: Eos (Transactions, American Geophysical Union) v. 87, no. 52, abs. T21B-0407.

Matti, J.C., Langenheim, V.E., Morton, D.M., Cox, B.F., and Landis, G.P., 2007, Late Neogene structural and stratigraphic relations in the Santa Rosa Mountains, southern California: Implications for Quaternary strain distribution in the southern San Andreas fault system: Southern California Earthquake Center Annual Meeting Abstracts.

McClay, K., and Bonora, M., 2001, Analog models of restraining stepovers in strike-slip fault systems: American Association of Petroleum Geologists Bulletin, v. 85, p. 233–260, doi:10.1306/8626C7AD-173B-11D7-8645000102C1865D.

McDougall, K., Poore, R.Z., and Matti, J.C., 1999, Age and environment of the Imperial Formation near San Gorgonio Pass, California: Journal of Foraminiferal Research, v. 29, p. 4–25.

McNabb, J.C., 2013, Stratigraphic record of Pliocene–Pleistocene basin evolution and deformation along the San Andreas fault, Mecca Hills, California [M.S. thesis]: Eugene, University of Oregon, 70 p.

Meade, B.J., and Hager, B.H., 2005, Block models of crustal motion in southern California constrained by GPS measurements: Journal of Geophysical Research, v. 110, B03403, doi:10.1029/2004JB003209.

Miller, M.S., Zhang, P., and Dolan, J.F., 2014, Moho structure across the San Jacinto fault zone: Insights into strain localization at depth: Lithosphere, v. 6, p. 43–47, doi:10.1130/L295.1.

Morton, D.M., and Matti, J.C., 1993, Extension and contraction within an evolving divergent strike-slip fault complex: The San Andreas and San Jacinto fault zones at their convergence in southern California, *in* Powell, R.E., et al., eds., The San Andreas fault system: Displacement, palinspastic reconstruction, and geologic evolution: Geological Society of America Memoir 178, p. 217–230, doi:10.1130/MEM178-p217.

Mueller, K., Kier, G., Rockwell, T., and Jones, C.H., 2009, Quaternary rift flank uplift of the Peninsular Ranges in Baja and southern California by removal of mantle lithosphere: Tectonics, v. 28, TC5003, doi:10.1029/2007TC002227.

Nicholson, C., Plesch, A., Shaw, J., Sorlein, C., and Hauksson, E., 2013, Updating the 3D fault set for the SCEC Community Fault Model (CFM-v4) and revising its associated fault database [poster]: Southern California Earthquake Center Annual Meeting 2013.

Persaud, P., Perez-Campos, X., and Clayton, R.W., 2007, Crustal thickness variations in the margins of the Gulf of California from receiver functions: Geophysical Journal International, v. 170, p. 687–699, doi:10.1111/j.1365-246X.2007.03412.x.

Plattner, C., Malservisi, R., Dixon, T.H., LaFemina, P., Sella, G.F., Fletcher, J., and Suarez-Vidal, F., 2007, New constraints on relative motion between the Pacific plate and Baja California microplate (Mexico) from GPS measurements: Geophysical Journal International, v. 170, p. 1373–1380, doi:10.1111/j.1365-246X.2007.03494.x.

Powell, C.L., II, 2008, Pliocene invertebrates from the Travertine Point outcrop of the Imperial Formation, Imperial County, California: U.S. Geological Survey Scientific Investigations Report 2008-5155, 25 p.

Powell, R.E., 1993, Balanced palinspastic reconstruction of pre-late Cenozoic paleogeology, southern California, *in* Powell, R.E., et al., eds., The San Andreas fault system: Displacement, palinspastic reconstruction, and geologic evolution: Geological Society of America Memoir 178, p. 1–106, doi:10.1130/MEM178-p1.

Rymer, M.J., 1991, Geological structure, transpression, and neotectonics of the San Andreas fault in the Salton Trough, California, Part 2: The Bishop ash bed in the Mecca Hills, *in* Wallawender, M.J., and Hannan, B.B., eds., Geological excursions in southern California and Mexico (Geological Society of America Annual Meeting Guidebook): San Diego, California, San Diego State University, p. 388–396.

Rymer, M.J., 1994, Quaternary fault-normal thrusting in the northwestern Mecca Hills, southern California, *in* McGill, S.F., and Ross, T.M., eds., Geological Investigations of an active margin (Geological Society of America Annual Meeting Guidebook): Redlands, California, San Bernardino County Museum, p. 325–329.

Saleeby, J., and Foster, Z., 2004, Topographic response to mantle lithosphere removal in the southern Sierra Nevada region, California: Geology, v. 32, p. 245–248, doi:10.1130/G19958.1.

Schmitt, A.K., and Hulen, J.B., 2008, Buried rhyolites within the active, high-temperature Salton Sea geothermal system: Journal of Volcanology and Geothermal Research, v. 178, p. 708–718, doi:10.1016/j.jvolgeores.2008.09.001.

Schmitt, A.K., and Vazquez, J.A., 2006, Alteration and remelting of nascent oceanic crust during continental rupture: Evidence from zircon geochemistry of rhyolites and xenoliths from the Salton Trough, California: Earth and Planetary Science Letters, v. 252, p. 260–274, doi:10.1016/j.epsl.2006.09.041.

Severson, L.K., 1987, Interpretation of shallow crustal structure of the Imperial Valley, California, from seismic reflection profiles [M.S. thesis]: Berkeley, University of California, Berkeley, 136 p.

Sharp, I.R., Gawthorpe, R.L., Armstrong, B., and Underhill, J.R., 2000, Propagation history and passive rotation of mesoscale normal faults: Implications for synrift stratigraphic development: Basin Research, v. 12, p. 285–305, doi:10.1046/j.1365-2117.2000.00132.x.

Sharp, R.V., 1967, San Jacinto fault zone in the Peninsular Ranges of southern California: Geological Society of America Bulletin, v. 78, p. 705–729, doi:10.1130/0016-7606(1967)78[705:SJFZIT]2.0.CO;2.

Sheridan, J.M., and Weldon, R.J., II, 1994, Accommodation of compression in the Mecca Hills, California, in McGill, S.F., and Ross, T.M., eds., Geological investigations of an active margin (Geological Society of America Annual Meeting Guidebook): Redlands, California, San Bernardino County Museum, p. 330–336.

Geosphere, published online on 27 August 2015 as doi:10.1130/GES01167.1

Shifflett, H., Gray, M.G., Grannell, R., and Ingram, B.L., 2002, New evidence on the slip rate, renewal time, and late Holocene surface displacement, southernmost San Andreas fault, Mecca Hills, California: Seismological Society of America Bulletin, v. 92, p. 2861–2877, doi: 10.1785/0120000601.

Shirvell, C.R., Stockli, D.F., Axen, G.J., and Grove, M., 2009, Miocene–Pliocene exhumation along the west Salton detachment fault, southern California, from (U-Th)/He thermochronometry of apatite and zircon: Tectonics, v. 28, TC2006, doi:10.1029/2007TC002172.

Sieh, K.E., and Williams, P.L., 1990, Behavior of the southernmost San Andreas fault during the past 330 years: Journal of Geophysical Research, v. 95, p. 6629–6645, doi:10.1029 /JB095iB05p06629.

Smith-Konter, B., and Sandwell, D.T., 2009, Stress evolution of the San Andreas fault system: Recurrence interval versus locking depth: Geophysical Research Letters, v. 36, L13304, doi: 10.1029/2009GL037235.

Sorichetta, A., Seeber, L., Taramelli, A., McHugh, C., and Cormier, M.H., 2010, Geomorphic evidence for tilting at a continental transform: The Karamursel Basin along the North Anatolian fault, Turkey: Geomorphology, v. 119, p. 221–231, doi:10.1016/j.geomorph.2010.03.035.

Spinler, J.C., Bennett, R.A., Anderson, M.L., McGill, S.F., Hreinsdóttir, S., and McCallister, A., 2010, Present-day strain accumulation and slip rates associated with southern San Andreas and eastern California shear zone faults from GPS: Journal of Geophysical Research, v. 115, B11407, doi:10.1029/2010JB007424.

Spotila, J.A., and Sieh, K., 2000, Architecture of transpressional thrust faulting in the San Bernardino Mountains, southern California, from deformation of a deeply weathered surface: Tectonics, v. 19, p. 589–615, doi:10.1029/1999TC001150.

Spotila, J.A., Farley, K.A., Yule, J.D., and Reiners, P.W., 2001, Near-field transpressive deformation along the San Andreas fault zone in southern California, based on exhumation constrained by (U-Th)/He dating: Journal of Geophysical Research, v. 106, no. B12, p. 30,909–30,922, doi:10.1029/2001JB000348.

Spotila, J.A., House, M.A., Blythe, A.E., Niemi, N., and Bank, G.C., 2002, Controls on the erosion and geomorphic evolution of the San Bernardino and San Gabriel Mountains, southern California, *in* Barth, A., ed., Contributions to crustal evolution of the southwestern United States: Geological Society of America Special Paper 365, p. 205–230, doi:10.1130/0-8137-2365-5.205.

Steely, A.N., Janecke, S.U., Dorsey, R.J., and Axen, G.J., 2009, Early Pleistocene initiation of the San Felipe fault zone, SW Salton Trough, during reorganization of the San Andreas fault system: Geological Society of America Bulletin, v. 121, p. 663–687, doi:10.1130/B26239.1.

Sylvester, A.G., and Smith, R.R., 1976, Tectonic transpression and basement-controlled deformation in San Andreas fault zone, Salton Trough, California: American Association of Petroleum Geologists Bulletin, v. 60, p. 2081–2102.

Sylvester, A.G., and Smith, R.R., 1987, Structure section in Painted Canyon, Mecca Hills, southern California, *in* Hill, M., ed., Centennial Field Guide 1—Cordilleran Section: Boulder, Colorado, Geological Society of America, p. 103–108.

Thornock, S.J., 2013, Southward continuation of the San Jacinto fault zone through and beneath the Extra and Elmore Ranch left-lateral fault arrays, southern California [M.S. thesis]: Logan, Utah State University, 178 p.

Todd, V.R., Erskine, B.G., and Morton, D.M., 1988, Metamorphic and tectonic evolution of the northern Peninsular Ranges Batholith, southern California, *in* Ernst, W.G., ed., Metamorphism and crustal evolution of the western United States: Rubey Volume VII: Englewood Cliffs, New Jersey, Prentice-Hall, p. 894–937.

U.S. Geological Survey and California Geological Survey, 2006, Quaternary fault and fold database for the United States, accessed February 22, 2012, from USGS web site: http://earthquakes.usgs.gov/regional/qfaults/.

Weldon, R.J., Meisling, K.E., and Alexander, J., 1993, A speculative history of the San Andreas fault in the Transverse Ranges, California, *in* Powell, R.E., et al., eds., The San Andreas fault system: Displacement, palinspastic reconstruction, and geologic evolution. Geological Society of America Memoir 178, p. 161–198, doi:10.1130/MEM178-p161.

Whipple, K.X., and Trayler, C.R., 1996, Tectonic control on fan size: The importance of spatially variable subsidence rates: Basin Research, v. 8, p. 351–366, doi:10.1046/j.1365-2117.1996 .00129.x.

Wilcox, R.E., Harding, T.P., and Seely, R., 1973, Basic wrench tectonics: American Association of Petroleum Geologists Bulletin, v. 57, p. 74–96.

Winker, C.D., 1987, Neogene stratigraphy of the Fish Creek–Vallecito section, southern California: Implications for early history of the northern Gulf of California and the Colorado Delta [Ph.D. thesis]: Tucson, University of Arizona, 622 p.

Winker, C.D., and Kidwell, S.M., 1986, Paleocurrent evidence for lateral displacement of the Pliocene Colorado River delta by the San Andreas fault system, southeastern California: Geology, v. 14, p. 788–791, doi:10.1130/0091-7613(1986)14<788:PEFLDO>2.0.CO;2.

Winker, C.D., and Kidwell, S.M., 1996, Stratigraphy of a marine rift basin: Neogene of the western Salton Trough, California, *in* Abbott, P.L., and Cooper, J.D., eds., Field conference guide 1996: Pacific Section, American Association of Petroleum Geologists Guidebook 73, p. 295–336.

Yule, D., and Sieh, K., 2003, Complexities of the San Andreas fault near San Gorgonio Pass: Implications for large earthquakes: Journal of Geophysical Research, v. 108, no. B11, p. 9-1–9-23, doi:10.1029/2001JB000451.

Zandt, G., Gilbert, H., Owens, T., Ducea, M., Saleeby, J., and Jones, C., 2004, Active foundering of a continental arc root beneath the southern Sierra Nevada, California: Nature, v. 431, p. 41–46, doi:10.1038/nature02847.

Geosphere

Crustal-scale tilting of the central Salton block, southern California

Rebecca J. Dorsey and Victoria E. Langenheim

Geosphere published online 27 August 2015;
doi: 10.1130/GES01167.1

Notes